Invited Review

Fundamental Aspects of Hot Isostatic Pressing: An Overview

H.V. ATKINSON and S. DAVIES

Hot isostatic pressing (hipping) can be used for upgrading castings, densifying presintered components, consolidating powders, and interfacial bonding. It involves the simultaneous application of a high pressure and elevated temperature in a specially constructed vessel. The pressure is applied with a gas (usually inert) and, so, is isostatic. Under these conditions of heat and pressure, internal pores or defects within a solid body collapse and diffusion bond. Encapsulated powder and sintered components alike are densified to give improved mechanical properties and a reduction in the scatter band of properties.

In this article, the basic science of sintering and hipping is summarized and contrasted. The current state of understanding and modeling of hipping is then reviewed. Models can be classified either as microscopic or macroscopic in their approach. In the microscopic approach, the various mechanisms of densification are analyzed in terms of a single particle and its surroundings. In the macroscopic approach, the compact is treated as a continuous medium. In hipping, although the pressure is isostatic, shrinkage is not generally isotropic, particularly if containment is used. However, the shrinkage can now be well predicted, provided that the material and container properties are accurately known.

I. INTRODUCTION

THE basics of hot isostatic pressing (hipping) have been summarized previously.[1,2,3] Hipping is largely concerned with the removal of pores. Pores may originate from, for example, the packing of powder particles, from gas evolution or shrinkage during the solidification of castings, from the agglomeration of vacancies generated by creep, and by interdiffusion during the bonding of dissimilar materials. The driving force to achieve densification is associated with the reduction in surface area and, hence, surface energy of the pores. The isostatic pressure in hipping arises from molecules or atoms of gas colliding with the surface of the object. Each gas atom is acting as an individual "hot forge." Under particular processing conditions, the gas atoms may be moving at a velocity of around 900 ms^{-1}, and approximately 10^{30} collision events are occurring per square meter per second. These tiny atomic forges reach all surfaces of the component, including re-entrant angles, and act reliably and consistently, independent of shape. On average, the number of gas atoms moving through a unit area, and their velocities, are the same in all directions. Thus, for every surface of a component that is being processed, the pressure is the same and acts in a direction normal to the surface.

Isostatic pressing must be distinguished from the more conventional unidirectional pressing. Pressure is applied along a single axis by a ram in unidirectional pressing, and the component is contained in a die. No intervening fluid is used to transmit the pressure; rather, it is transmitted by contact between the solid surfaces of the ram and the die and the component under pressure. Since friction exists between the object and the die walls, this contributes to a variation in pressure with position in the compact and, hence, to nonuniform densification. There are no such problems with isostatic pressing. There are no rams, dies, or external frictional forces.

When consolidating a powder to develop a specified shape and size, the powder is first placed into a can or envelope of the same shape as that specified, but of a larger overall size. The envelope must be made from a material (such as metal or glass) that can deform in a plastic manner at the temperature and pressure of the appropriate hipping treatment. As densification occurs, the powder compact shrinks. The external metal or glass envelope shrinks with it to the same extent in all directions (subject to certain limitations, which will be discussed in Section III) because the pressure is isostatic. Hence, the densifying powder is formed into the same shape as the envelope. Essentially, the envelope and powder undergo a photographic reduction in shape (Figure 1).

A uniform photographic reduction in shape cannot easily be achieved with unidirectional pressing of powders, nor can unidirectional pressing fully remove internal voids from preformed components. In contrast, total void removal can be achieved by hipping, and it is the isostatic nature of the pressure which allows preformed complex shapes (*e.g.*, those of turbine discs) to be maintained during the process.

Typical hipping pressures and temperatures for various materials are shown in Table I (a more detailed table is given in Reference 4) for comparison with yield stress at room temperature and at the melting point (T_m). A typical hipping pressure of 100 MPa (approximately 1000 atm) is roughly equivalent to the pressure at the bottom of the ocean's deepest trench. The gas pressure developed during a hipping cycle is achieved partly by a mechanical compressor and partly by heating the gas in a closed space (*i.e.*, at constant volume). The relationship of pressure to temperature expressed in the ideal-gas laws starts to break down at very high pressures, but, even so, as the temperature rises, the pressure at a fixed volume must also increase.

The temperatures for hipping are usually greater than 0.7

Dr. H.V. ATKINSON is with the Department of Engineering Materials, The University of Sheffield, Sheffield, S1 3JD, United Kingdom. S. DAVIES, Business Development Manager, is with Bodycote HIP Limited, Chesterfield, S41 9ED, United Kingdom.

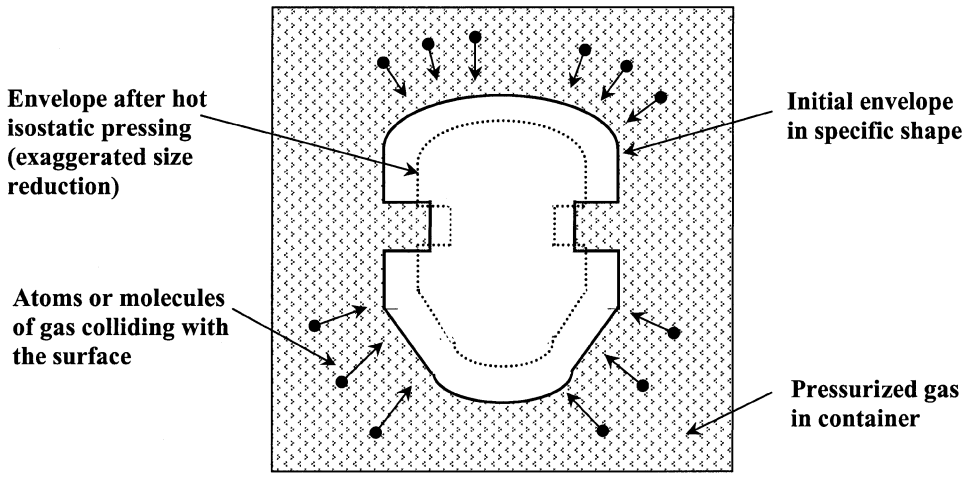

Fig. 1—Isostatic pressing causes a photographic reduction in the shape of an encapsulating envelope and the densifying powder that it contains.

Table I. Typical Hipping Pressures and Temperatures

Material	Melting Point T_m (°C)	Yield Stress at Room Temperature (MPa)	Hipping Temperature (°C)	Hipping Pressure (MPa)
Al and its alloys	660 (Al)	100 to 627	500	100
Al/Al_2O_3	—	—	300	350
Cu and its alloys	1083 (Cu)	60 to 960	800 to 950	100
Be and its alloys	1289 (Be)	240	900	103
Nimonic and superalloys	1453 (Ni)	200 to 1600	1100 to 1280	100 to 140
Hydroxyapatite	—	—	1100	200
Mg/Zn ferrite	—	—	1200	100
TiAl	—	—	900 to 1150	35 to 200
Ti_3Al	—	—	925	200
Ceramic superconductors	—	—	900	100
Steels	1536 (Fe)	500 to 1980*	950 to 1160	100
Ti and its alloys	1670 (Ti)	180 to 1320	920	100
Al_2O_3	2050	5000	1500	100
Al_2O_3/glass	—	—	1400	100
Al_2O_3/TiC	—	—	1935	150
Al_2O_3/ZrO_2	—	—	1500	200
SiC	2837	10,000	1850	200
B_4C	—	—	2000	200
WC/Co	2867	6000	1350	100

*Low-alloy steels (water quenched and tempered).

T_m. For example, cast superalloy turbine blades are processed in the temperature range from 1100 °C to 1280 °C. Some materials may contain a relatively low-melting-point constituent that aids pore removal, if the hipping is carried out between the melting point of this constituent and that of the matrix. The relatively high temperatures during hipping are necessary to lower the yield strength and to raise the diffusivities in the material sufficiently for pore closure to occur in a reasonable time. Considerable engineering demands are placed on hot-isostatic-press processing equipment by the combination of elevated temperature, high pressure, and time.

The hipping process was originally developed[5] for diffusion bonding of nuclear reactor components and for the removal of porosity in hard materials (*e.g.*, Reference 6). However, the major commercial activity now centers upon the consolidation of metal powders and on the densification of high-performance castings. Hipping is utilized in a wide range of industries, including aerospace, marine and offshore, power generation, automotive, medical, defense, microelectronics, telecommunications, metal working, and mining. Table II shows a number of applications of hipping together with typical examples of materials. The applications in Table II essentially represent a spectrum in terms of percentage porosity removed by the hipping process.

Hipping can remove both macro- and microporosity. Microporosity develops in castings owing to shrinkage effects and gas evolution as the molten metal cools and becomes solid. The static and dynamic mechanical properties of castings (*e.g.*, strength, creep, toughness, and fatigue) are adversely affected by the presence of microporosity (*e.g.*, for toughness, refer to Figure 2). Traditionally, casting pores

Table II. Applications of Hipping: Aims and Examples of Materials Processed

Application	Primary Aim	Materials
Densification of castings	to remove macroporosity and microporosity	Ni- and Co-based superalloys Ti alloys Al alloys steels Cu alloys
Densification of presintered powders	to achieve full theoretical density and to avoid excessive grain growth (difficult by conventional methods)	WC-based hardmetals Si_3N_4, Al_2O_3, ZrO_2, and other advanced ceramics Be alloys
Consolidation of encapsulated powders	to achieve full theoretical density and to avoid segregation and excessive grain growth	high-speed tool steel ceramics metal matrix composites (*e.g.*, Al-SiC) ceramic-ceramic composites magnetic materials (*e.g.*, ferrites) ceramic superconductors Fe-TiC
Interface bonding	to diffusion bond similar and dissimilar materials (overcoming problems of conventional joining and uniaxial diffusion bonding techniques) to bond and densify coatings	bronze and steel Ni alloys and steel ceramic-metal bonding Ta, Ti, Al, and W in Al housing for sputter targets
Specialized applications	to remove pores and gaseous impurities from optical materials	ZnS Sn-In-O lanthanates and aluminates
Reactive hipping	to synthesize compounds by exothermic reaction during heating at hot isostatic press temperature	intermetallics, *e.g.*, TiB_2 and Nb_3Al

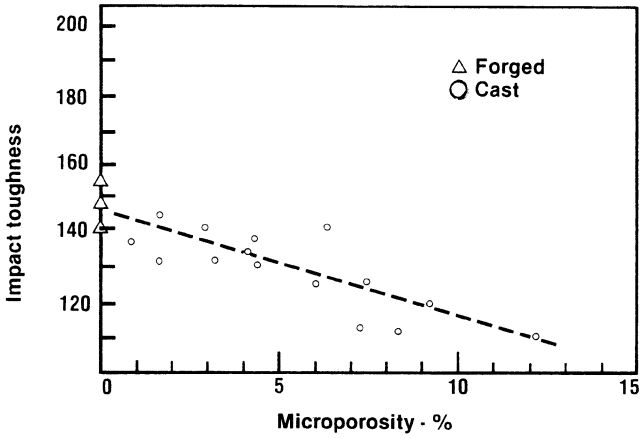

Fig. 2—Influence of microporosity on impact toughness (J/cm^2) of 1 wt pct Cr-0.25 wt pct Mo cast steel.[7]

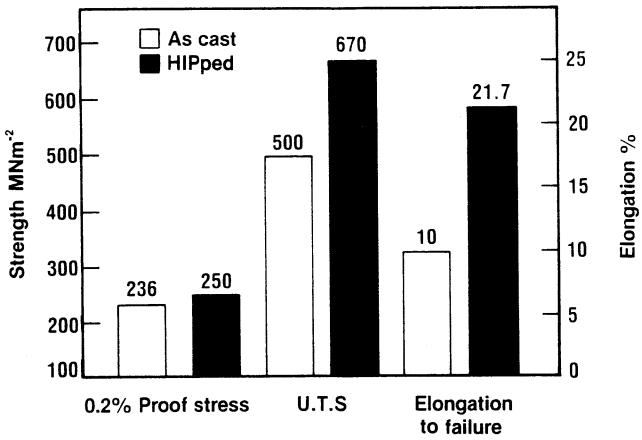

Fig. 3—Mechanical properties of Ni-Al bronze (AB2) containing 10 to 20 pct porosity, in the as-cast and hipped conditions. UTS = ultimate tensile strength. (Data from Dr. B.A. Rickinson at HIP Ltd.)

have been removed by hot working, *e.g.*, by forging, but this adds to the cost and changes the shape.

Any technique such as hipping, which can be used to remove porosity while not adversely affecting the microstructure (*i.e.*, grain structure, phases present, and precipitate arrangement), is of considerable significance, both for improving reliability in service and for reducing scrap rates during manufacture. Indeed, hipping can influence the microstructure beneficially.[8] Figure 3 shows a typical improvement in strength and elongation to failure, Figure 4 shows a typical improvement in fatigue life, and Figure 5 shows a typical improvement in creep life. The properties after hipping can be comparable with those of forged components.

Hipping not only improves average mechanical properties but also can have an important benefit in reducing the property scatter (*e.g.*, References 10 and 11). When a number of specimens are tested, a range of values may be obtained, scattered about the average (Figure 6). After hipping, the average is improved and, perhaps more importantly, the width of the distribution is decreased. This is particularly important where fatigue and creep lives must be predicted as accurately as possible, so as to schedule maintenance accordingly. In addition, the enhancement in minimum property levels due to hipping provides the means by which the designer can work confidently with higher design values.

The structure of the overview is as follows. In Section II, the basic science of sintering is summarized and contrasted with that for hipping. The mechanisms and stages of pore

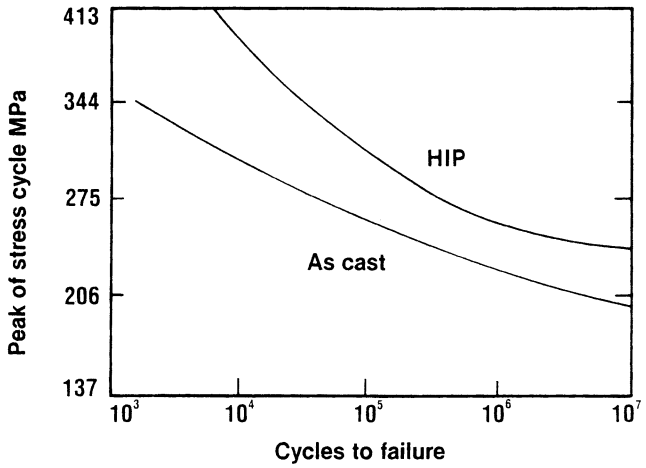

Fig. 4—Effect of hipping on fatigue life of Ti-6 wt pct Al-4 wt pct V at 316 °C.[9]

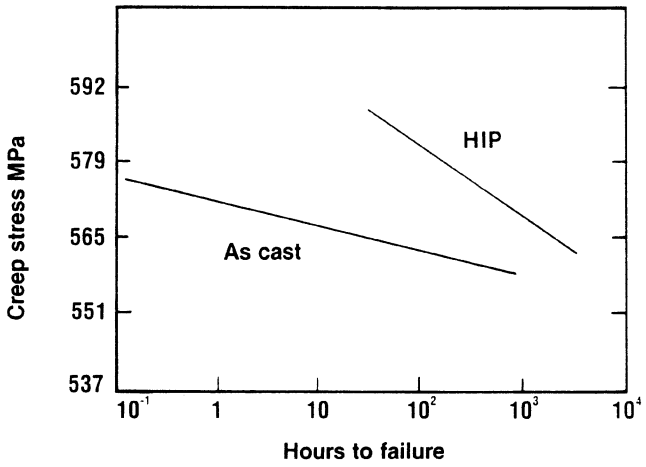

Fig. 5—Influence of hipping on creep life of Ti-6 wt Al-4 wt pct V at 399 °C.[9]

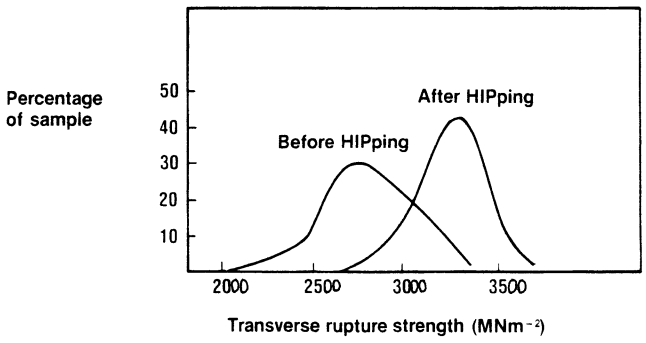

Fig. 6—Transverse rupture strength of tungsten carbide hard-metal specimens (WC 3.5-μm 11 pct Co) before and after hipping, illustrating increase in the average strength and reduction in data scatter with hipping.[10]

closure (*i.e.*, densification) during sintering, *i.e.*, when heat is applied but no pressure, are considered. When pressure is applied in addition to heat, the densification mechanisms are modified. Densification mechanisms are then dependent on the pressure, the temperature, the pore size, and the location of the pores. The potential effects of hipping on the microstructure and segregation are discussed, and the problems presented by surface-connected porosity are also highlighted here. Such porosity cannot be removed by a simple hipping treatment and, to achieve full density, it is important to minimize the surface connection. It is possible to overcome such limitations by the use of surface coatings or encapsulation.

Section III deals with the modeling of hipping, differentiating between microscopic models and the macroscopic approach. For the microscopic approach, various workers have developed models to deal with deviations from the original assumptions, *i.e.*, ranges of particle sizes, nonspherical particles, non-steady-state pressure and temperature, anisotropic shrinkage, and hipping of composites. The macroscopic approach has been particularly used in conjunction with finite-element modeling. The prediction of anisotropic shrinkage is a major aim. In Section IV, recent developments in the modeling of the effects of hipping on microstructure, the use of *in-situ* sensors, and the role of densification during the initial transient and reactive hipping are summarized. Concluding remarks are then given. The focus of this review is the fundamental science of hipping. The reader is directed elsewhere for further detail on the practice and its applications (*e.g.*, References 3 and 4).

II. SINTERING AND HIPPING

A. *Sintering*

Sintering occurs when heat is applied to a powder or to a body containing pores. Formal theories for pore removal and sintering of grain-boundary cavities have been reviewed.[4,12] The driving force for sintering is the reduction in the surface area associated with pores. The surface area of fine powders is considerable. For example, a cupful of powder with a particle size of 1 μm has a surface area of approximately 10^3 m^2. If the surface energy of the powder material is approximately 1 J m^{-2} (a typical value), the surface energy of the cupful of powder is, therefore, about 1 kJ.

Grain boundaries and dislocations are also regions of disorder and, therefore, are zones of high energy relative to the perfect crystal in the bulk. All systems try to achieve their minimum energy configuration and, in the limit, for a crystalline material, this is a single crystal containing no defects (pores, grain boundaries, dislocations, *etc.*) whatsoever. From a thermodynamic standpoint, the first step toward the goal of reduced energy is for pores to be eliminated from the system (the specific surface energy of pores is greater than the grain-boundary energy). However, during any sintering activity, the process of grain-boundary elimination (grain growth) often begins before the process of pore elimination has been completed. This state can then inhibit further pore removal for mechanistic reasons (see later in this section).

The driving force for closure of an isolated spherical pore can be expressed[13] in terms of the pressure (p), such that

$$p = \frac{2\gamma}{r} \qquad [1]$$

where γ is the specific energy (in joules per square metre) of the internal surface of the pore and r is the radius of curvature of the pore surface. For a spherical pore, r is the

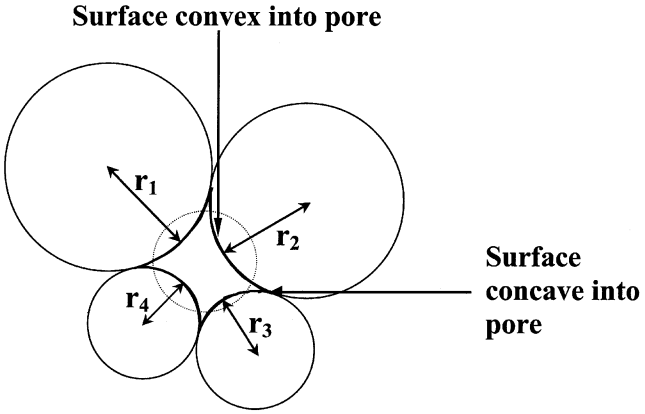

Fig. 7—Pore between powder particles with varying radii of curvature around the pore surface. The broken curve shows the pore surface after some spheroidization has taken place by redistribution of material from convex neck surfaces to concave powder particle surfaces.

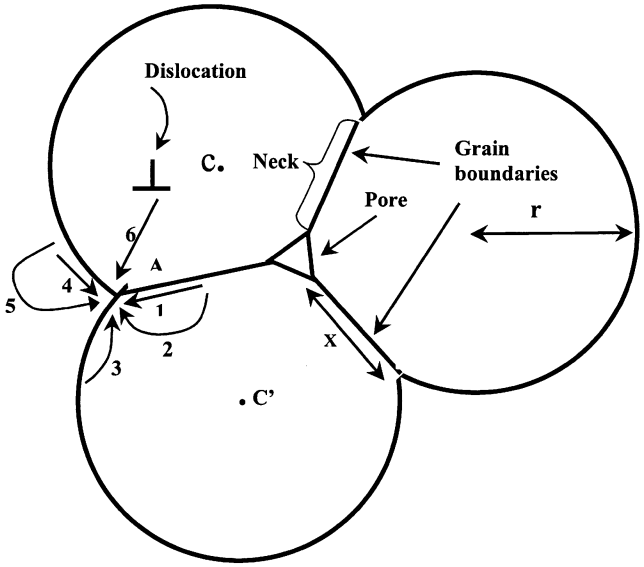

Fig. 8—Paths for transport of matter during neck growth in sintering (Table III gives transport paths to which numbers correspond). *C* and *C′* are the particle centers, *X* is the neck diameter, and *r* is the particle radius.

radius of the sphere, but, for a more irregularly shaped pore, the surface can be divided into a number of regions with different radii of curvature (Figure 7). Where the surface is concave into the pore, the radius is taken to be positive, and where the surface is convex, the radius is negative.

Two important points emerge from Eq. [1]. The first is that the driving force for the removal of small pores is greater than that for the removal of larger pores. Using the equation, the driving force for a pore of 1 mm in diameter is 4×10^{-3} MPa and that for a 1 μm pore is 4 MPa. It, therefore, tends to be the larger pores which remain toward the end of the diffusion process.

The internal porosity in many castings arises from the precipitation of gas.[14] The internal pressure of the gas will tend to oppose the driving force for shrinkage.[15] As a pore shrinks, the internal pressure of the gas will rise. The gas may then tend to dissolve into the matrix[16] and diffuse to a region of lower pressure, *i.e.*, to larger pores or to the surface of the component. Thus, large pores grow at the expense of smaller pores. For an irregularly shaped pore, matter will tend to be transported to concave regions of small radius of curvature (*i.e.*, tight curves) from those where the surface is more gently rounded or convex (Figure 7). Thus, irregularly shaped pores tend to spheroidize. It should be noted that pores in solids are often faceted, because certain crystallographic planes have lower surface energies than others.[17] This tendency to spheroidize is counteracted by the fact that, where a pore sits at the meeting of two, three, or four grains, then, provided that thermodynamic equilibrium is achieved, the geometry will be determined by the various interfacial energies.[18,19]

The diffusional mechanisms for removal of pores (including vapor transport) in sintering are summarized in Figure 8, and the transport paths are identified in Table III.[20,21,22] Matter can be transported to fill a pore at point A in Figure 8 from a grain boundary between two particles (*via* the grain boundary itself or the lattice) or from dislocations within the particles (*via* the lattice). These transport paths correspond to paths 1, 2, and 6 in Table III and bring the centers of the particles (*C* and *C′*) closer together. They, therefore, result in densification. By way of contrast, paths 3 through 5 do not cause densification, because they only involve the transport of matter from one place on the surface of the pore to another. The net result is a change in the shape of the pore, but no change in its volume. It can be seen in Figure 8 that, as the pore is filled at point A, the length of the neck between the two particles grows.

Table III. Diffusion and Vapor Transport Paths and Sources for Matter in Sintering (the Sink in Each Case Is the Neck)

Mechanism	Transport Path	Source of Matter
1	grain boundary diffusion	grain boundary
2	lattice diffusion	grain boundary
3	lattice diffusion	surface
4	surface diffusion	surface
5	vapor transport	surface
6	lattice diffusion	dislocation

In addition to the transport paths identified previously, viscous and plastic flow may also occur along with particle rearrangement. Viscous flow is important in the sintering of glasses and other amorphous materials. The occurrence of plastic flow in crystalline materials during sintering, *i.e.*, the transport of relatively large numbers of atoms by dislocation slip, has been controversial. For plastic flow to occur, the stresses must be high enough for new dislocations to be generated. During sintering without the application of external pressure, this is probably only possible in the very initial stages of contact formation. There is evidence of densification-rate improvements due to dislocation climb.[23]

Of the paths identified in Figure 8 and Table III, apart from path 5, which involves vapor transport, the other paths all involve diffusion *via* the pore surface, the grain boundaries, or the lattice. (Diffusion along dislocation pipes in the grains may also occur.) Diffusion is thermally activated. Surfaces are regions of relatively high disorder, and, therefore, the activation energy for diffusion tends to be low. The activation energy in grain boundaries is generally higher, and that in the lattice is higher still. Hence, at low temperatures, surface diffusion dominates over grain-boundary and lattice

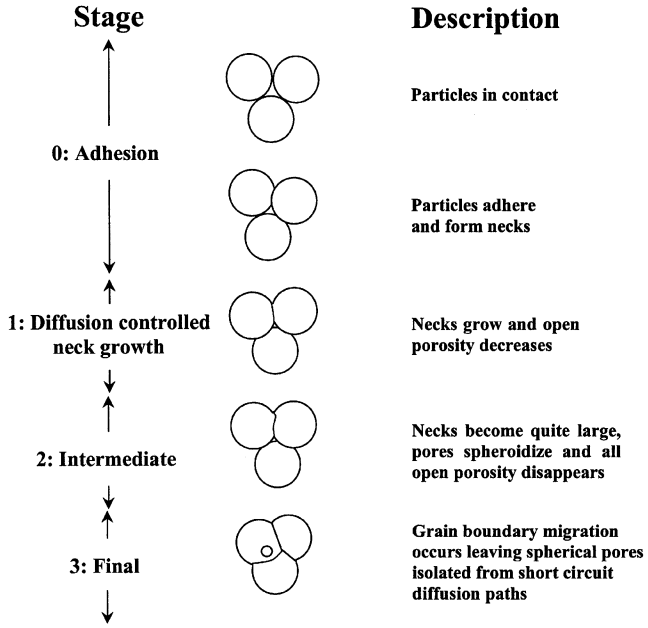

Fig. 9—Stages of sintering.

diffusion. As the temperature is increased, grain-boundary diffusion predominates and, at higher temperatures, lattice diffusion becomes the principal route for diffusion. The change from one predominating mechanism to another depends on the cross-sectional area of the short-circuit paths (*i.e.*, grain boundaries and surfaces) available. If the material has a fine grain size, the cross-sectional area of short-circuit paths will be high, and lattice diffusion will only be prevalent at relatively high temperatures.

The stages of sintering are shown in Figure 9. In the final stage, the pores are spherical. Grain-boundary migration can occur to minimize grain-boundary energy, leaving pores isolated from grain-boundary diffusion routes. Removal of such isolated pores is then relatively slow, as transport must occur through the lattice.[24] Therefore, if full density is to be achieved, it is important that grain-boundary migration be avoided. Second-phase particles and impurities can help to pin grain boundaries. Pores themselves also pin boundaries, and it is in the latter stages, when some pores are totally eliminated, that the boundaries can break free from surviving pores and migrate to lower-energy configurations.[25] The strength of pinning increases with the decrease in size of the pores or particles.

There are various methods to enhance densification during sintering of powders without the use of external pressure. These include "liquid-phase" sintering; "reactive liquid" sintering and "reaction bonding;" and "transient liquid-phase" sintering and "activated sintering." Liquid-phase sintering, for example, may limit the temperature at which the component is used if the low-melting-point constituent is still present.

Densification can, to a certain extent, be achieved for some materials by the application of pressure alone. This is the process occurring in cold isostatic pressing (cipping). The slower the compaction speed, the more particle rearrangement is allowed to occur and the faster the theoretical density (*i.e.*, zero porosity) is approached. Soft particles can deform into pores more easily than harder particles can and, again, the rate of approach to theoretical density is accelerated. The pressure causes particle rearrangement by slippage and restacking, elastic and plastic deformation at contact points, and cold working of ductile particles. Brittle particles may fracture under the imposed stress, leading to comminution. At the contact points, the heat generated by friction may be sufficiently high for local melting to occur. On resolidification, the particles are welded together across the interface. High local stress can also lead to recrystallization across contact points, again effectively giving local welding. Welding at contact points can frustrate the achievement of the theoretical density, because further particle rearrangement is then inhibited.

B. *2.2 Hot Isostatic Pressing*

The combination of pressure and temperature can be used to achieve a particular density at a lower temperature than would be required for sintering alone[26] and at a lower pressure than required for cipping. The effect of the lower temperature is that unacceptable grain growth can be avoided. In addition, the methods identified previously for enhancing densification of powders by introducing additives such as low-melting-point constituents (which may have deleterious effects on mechanical properties) are not needed.

The surface-energy driving force for pore closure, and the opposition to it caused by gas in pores, have already been mentioned. For a pore of 0.1 mm in diameter, the driving force for closure (from Eq. [1], with $\gamma = 1$ J m^{-2}) is 40 kPa. In hipping, however, the external pressure of, for example, 100 MPa adds to and completely swamps this driving force and almost inexorably causes any gas in a pore to dissolve into the matrix. Gases in pores (*e.g.*, from casting) are invariably soluble (in contrast with the argon used for pressurization in hipping) and the solubility of such gases increases with the increasing pressure within the pore, which increases during the early stages of hipping. Under pressure, the gas diffuses to the surface rather than to another pore, as in sintering. The pore then collapses. It is only when a pore reduces to a diameter of perhaps 40 nm that the driving force due to surface energy becomes comparable to that due to the externally applied pressure.

One potential difficulty with hipping is thermally induced porosity. The high external pressure collapses gas-filled pores and gives full density. However, during subsequent heating without pressure, swelling can occur as gas establishes an equilibrium pressure dependent on the surface energy. Thus, it is important to minimize the gas in closed pores by degassing the compact and avoiding temperatures where one of the species can decompose or react to create a vapor. This can be done by vacuum sintering to the closed-pore condition, prior to pressurization, to avoid trapped gas.

Yield stresses decrease, for most metals and ceramics, with increasing temperatures. The hipping conditions are generally chosen so that the gas pressure is greater than the reduced yield point of the material at that temperature. Plastic flow can then occur on a microscopic scale. Under hipping conditions, considerable particle shear occurs, and creep processes such as Nabarro–Herring creep (diffusion through grain interiors), Coble creep (diffusion around grain boundaries), and dislocation creep operate at relatively high rates. For glasses and other amorphous materials, densification is by viscous flow.[27] For some ceramics, such as lead zirconate

titanate, pressure-enhanced grain rearrangement and solution precipitation are the processes primarily responsible for densification.[28] Particle shear on extrusion can break up surface films on particles (*e.g.*, oxides), exposing new clean surfaces and, hence, enhancing surface diffusion rates. Some fine oxide particles may be retained after hipping, and decoration of prior powder-particle boundaries may occur, leading to degraded mechanical properties. Rapid-solidification technology in powder fabrication and clean handling procedures to avoid contamination prior to consolidation can alleviate these difficulties. In cold pressing, densification is retarded by the effects of work hardening within particles but, with hot pressing, the dislocation tangles and pileups are constantly eliminated so that particles can continue to deform.

During the final stages of hipping densification, when only isolated pores are present, the surfaces of the pores are not simply pushed together to develop a planar crack. Bonding occurs, because atoms diffuse in both directions across the interface (a microscopic form of the diffusion bonding). At this stage, pore dimensions are small (1 μm or less) and the sustain time (1 hour or longer) is more than adequate to allow complete closure.

The major effects of hipping on microstructure are the removal of porosity and grain growth. Changes in precipitate distributions and changes in segregation patterns must also be considered. For example, Smugeresky[29] found that after hipping a ferrous alloy, it tended to fracture along the prior particle boundaries. This occurred because titanium was segregating to the prior particle boundaries during processing, leading to low toughness in the densified product. Changes in precipitate distributions and changes in segregation patterns involve diffusion and are, therefore, enhanced at high temperatures. In addition, the high pressures might influence phase transformations, change melting points, and crack brittle particles.

The higher the temperature, the more rapid the grain-boundary migration. Boundaries can be pinned by impurities or by fine distributions of precipitates. However, as the temperature increases, impurity diffusion is enhanced and precipitates may coarsen or dissolve, allowing boundaries to migrate. The effect of precipitates in pinning dislocations is also then reduced, hence, decreasing the yield stress. All these major processes occur with conventional sintering as well as hipping, but the advantage of hipping is that the temperatures required for densification are lower and the times at elevated temperature are shorter. Excessive grain growth can then be avoided, thereby retaining the relatively high yield strengths and toughnesses which fine grain sizes confer.

Segregation can be a serious problem in casting. The temperatures involved in hipping allow segregants to diffuse, evening out chemical profiles on the microscale and, so, enhancing properties. Normal hipping cycles are not usually sufficiently prolonged for macrosegregation across an ingot to be removed, but, even so, compositional profiles will be smoothed.

The pressures involved in hipping (typically 100 MPa) tend to be too low in and of themselves to cause phase transformations. (For example, graphite can be transformed to diamond at 1000 °C by about 2500 MPa pressure.) Phase transformations have not, therefore, been generally regarded as a serious concern in hipping, although transformations between metastable phases (*e.g.*, from a glassy state to the crystalline state of a ceramic) might be initiated by pressure. For materials that shrink on solidification (*i.e.*, the majority), pressure will raise the melting point. This effect is small, a few degrees Celsius at most.

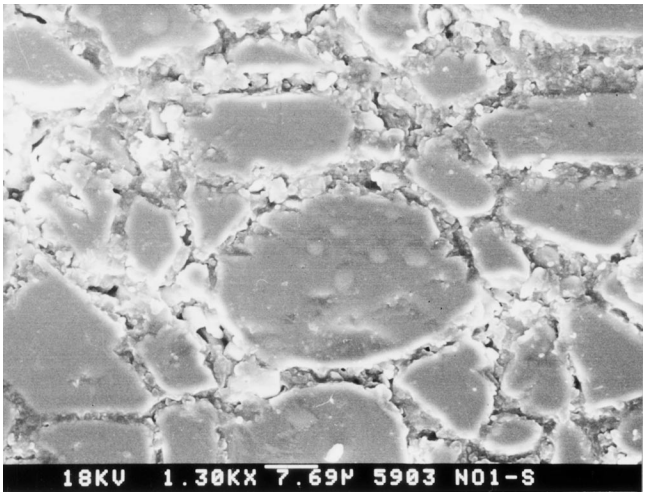

Fig. 10—Alumina sample after hipping at 1850 °C/12 MPa/1 h. The microstructure shows the fragments of material in what was originally a pore 4 mm in radius before hipping (courtesy of Drs. Sangho Lee, Jae Kyun Yang, and Doh-Yeon Kim).

Hipping pressures can also crack those brittle particles associated with porosity in ductile matrices. Such effects can, in fact, be favorable, but underline the need for careful control of pressure and temperature ramp rates.

The relationship between cost and hipping conditions (temperature, pressure, and time) is not simple. The shortest cycle is not necessarily the cheapest. In addition, potential effects on the microstructure must be taken into account. In general, the processing temperature (T) is greater than 0.7 T_m, where T_m is the solidus. Typical examples of hipping conditions are given in Table I. For brittle ceramics, particular care must be taken to ensure that hipping is carried out in a pressure/temperature regime where the material exhibits extensive plastic deformation without inducing crack propagation. Al_20_3 specimens containing artificially large (4 mm radius, for example) spherical pores have been used to demonstrate that such pores can be removed by a regime of 1850 °C/12 MPa/15 min followed by 1850 °C/50 MPa/30 min (*i.e.*, low pressure followed by high pressure), but not by applying high pressure (50 MPa) immediately on heating.[30] These and similar specimens also graphically demonstrated the dynamic nature of some pore-removal mechanisms, with particle fragments being created as grains flow into the large pore (Figure 10). The whole of the area shown in Figure 10 was originally the interior of a large pore. With the application of temperature and pressure, the area now contains fragments of Al_20_3. With further treatment, the particle fragments are consumed by grain growth. There have been recent moves toward reducing cycle times through hipping at higher pressures (up to 515 MPa) than those conventionally used. For metals and intermetallics, which densify by plasticity/power-law creep, higher pressures will lead to accelerated densification. However, for ceramics, which often densify through diffusional creep, the low thermal conductivity can limit pressurization and depressurization rates because of

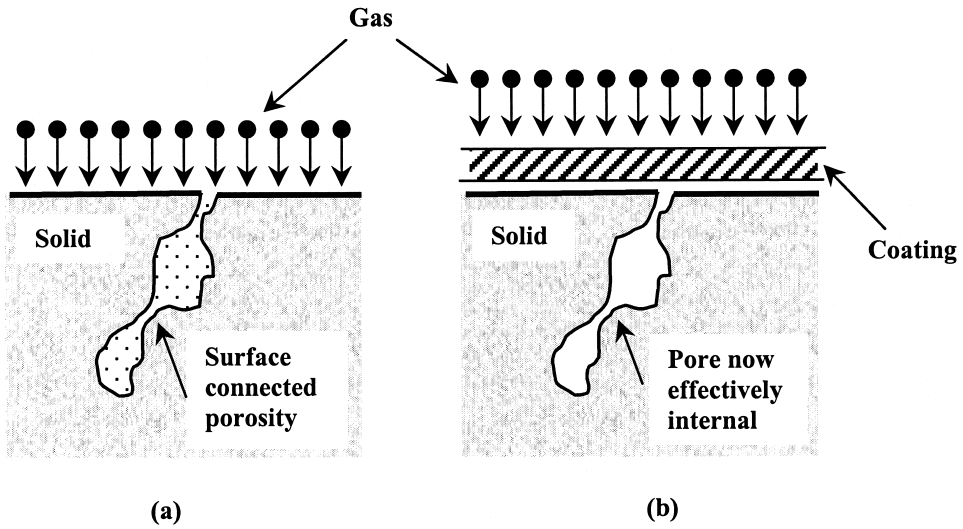

Fig. 11—Surface-connected porosity and its counteraction by coating or encapsulation. (*a*) The pressurizing medium impinges on the surface-connected porosity as though it were an extension of the surface. (*b*) After coating, the surface-connected porosity effectively becomes internal and can be closed if the pores are evacuated.

the risk of thermal cracking. In addition, for some materials, shorter cycle times may not be advantageous (*e.g.*, for castings, shorter cycle times lead to reduced homogenization). Models and the hipping diagrams that arise from them (as discussed in Section III) can simplify and guide the choice of temperature and pressure for hipping.

The pressurizing gas medium impinges on surface-connected porosity as though it were an extension of the surface of the object. Such porosity is, therefore, not removed by hipping (Figure 11(a)). However, surface-connected pores can be critical defects in many applications (*e.g.*, dies and rolls), and steps must be taken to minimize such surface connections. If the object is coated or encapsulated, the surface-connected porosity effectively becomes the internal porosity (Figure 11(b)) and is removed by the hipping treatment. The coating or encapsulating material can then be subsequently machined or dissolved off.

One route to avoid the need for encapsulation is to presinter to a state of closed porosity. This can either be done in separate vessels (sinter + hot isostatic press) or in the same vessel (sinter-hot isostatic press). The latter process has been increasingly used in recent years for a variety of materials, particularly for ceramics such as Si_3N_4, sialons, Al_20_3, and glass-ceramic composites. The composition of the atmosphere can be better controlled by the sinter-hot isostatic press process than by the sinter + hot isostatic press process, to avoid potential volatilization of constituents or decomposition effects. Depending on the ceramic under consideration, very small additions of carbon, nitrogen, or oxygen to the high-purity argon must be made. Thus, ceramics or ceramic superconductors can be processed in an oxidizing atmosphere. The difficulty with the sinter-hot isostatic press process is that the equipment required is highly specialized, requiring, for example, a dewaxing/debinding facility as an integral feature and a facility to change the atmosphere during heating. The process has only been developed for certain specialized applications.

III. MODELING OF HIPPING

Since the applied load (gas pressure) is hydrostatic, the deformation of the porous body is supposed to be isotropic. In practice, the initial and final products differ in scale, but also in shape. The factors controlling shrinkage are complex and depend on many variables: process parameters (temperature, pressure, etc.) and material properties (*e.g.*, powder particle size, creep, and diffusion constants). This precludes prediction using simple calculations. Trial and error in container design is expensive and time consuming.

Modeling is, thus, essential in order to achieve better performance of the industrial process; control the quality and properties of the products; predict the final shape; optimize the process; limit costs; and obtain a better understanding. It must take into account the fact that hipping is a thermomechanical process, with consolidation and heat transfer occurring simultaneously during the heating (and cooling). Li and Haggblad[31] have recently summarized the two different types of models: microscopic and macroscopic.

A. *Microscopic Models*

The microscopic approach was pioneered by Wilkinson,[32] Ashby and co-workers,[33,35,36] and Arzt[34] and was built on foundations laid, for example, by Gilman and Gessinger.[37] It essentially has its roots in sintering theory and concentrates on the local behavior of particle necks. The various mechanisms of densification (power-law creep, vacancy diffusion, etc.) are analyzed in terms of a single particle and its surroundings.

For the various hot isostatic press mechanisms, constitutive equations have been developed which predict the contribution of each mechanism to densification. They are based on the physical principles that describe the evolution of the process and require certain simplifying assumptions to be made to allow a tractable mathematical treatment. The powder particles are assumed to be equally sized, spherical, and

Table IV. Summary of Equations for Hot Isostatic Press Densification Rate $\dot{D}$ and Effective Pressures P_{eff}[38]

Mechanism/Stage	Equation	Reference
Plastic yield		
Stage 1	$D_y = \left(\frac{(1 - D_0)P}{1.3\sigma_y} + D_0^3\right)^{1/3}$	36
Stage 2	$D_y = 1 - \exp\left(\frac{-3\left(P - P_0\frac{(1 - D_c)D}{(1 - D_y)D_c}\right)}{2\sigma_y}\right)$	36
Power-law creep		
Stage 1	$\dot{D} = 5.3(D^2D_0)^{1/3}\frac{1}{\sqrt{3}}\left(\frac{D - D_0}{1 - D_0}\right)^{1/2} A\left(\frac{P_{1eff}}{3}\right)^n$	35, 36
Stage 2	$\dot{D} = \frac{3}{2}A\frac{D(1 - D)}{(1 - (1 - D)^{1/n})}n\left(\frac{P_{1eff}}{2n}\right)^n$	22, 35, 36
Boundary diffusion		
Stage 1	$\dot{D} = 43\left(\frac{1 - D_0}{D - D_0}\right)\frac{\delta D_b}{R^3}P_{1eff}\frac{\Omega}{k_BT}$	36
Stage 2	$\dot{D} = 4\frac{\delta D_b}{R^3}P_{2eff}\frac{\Omega}{k_BT}$	46
Volume diffusion		
Stage 1	$\dot{D} = 32(1 - D_0)\frac{D_v}{R^2}P_{1eff}\frac{\Omega}{k_BT}$	36
Stage 2	$\dot{D} = 3\left(\frac{1 - D}{6D}\right)^{1/2}\frac{D_v}{R^2}P_{2eff}\frac{\Omega}{k_BT}$	19
Diffusional flow		
Stage 1	$\dot{D} = \frac{14.3}{D}\left(\frac{1 - D_0}{D - D_0}\right)^{1/2}\left(\frac{D_v}{G^2} + \frac{\pi\delta D_b}{G^3}\right)\frac{\Omega}{k_BT}P_{1eff}$	19, 36
Stage 2	$\dot{D} = 32(1 - D)\left(\frac{D_v}{G^2} + \frac{\pi\delta D_b}{G^3}\right)\frac{\Omega}{k_BT}P_{2eff}$	19, 36
Effective pressures		
Stage 1	$P_{1eff} = \frac{P(1 - D_0)}{D^2(D - D_0)} + \frac{3\gamma_{sv}}{R}D^2\left(\frac{2D - D_0}{1 - D_0}\right)$	36
Stage 2	$P_{2eff} = P + \frac{2\gamma_{sv}}{R}\left(\frac{6D}{1 - D}\right)^{1/3} - P_0\frac{(1 - D_c)D}{(1 - D)D_c}$	36

arranged in a random dense packing. The hipping pressure and temperature are assumed to be in steady state and the shrinkage to be isotropic. Densification is continuous, but, owing to the extent of the geometry changes, it is convenient to split it into two stages, the first with open porosity and the second with closed. During stage 1 (typically, a relative density of <0.9), the particles are discrete and touch at necks. Stage 2 (typically, a relative density of >0.9) begins when the porosity ceases to be connected.[35,36] Densification-rate equations are summarized in Table IV.[38] The symbols used in Table IV are defined in Table V. The total densification rate is given by summing the densification rates for each of the processes of power-law creep, boundary diffusion, volume diffusion, and diffusional flow.

As in the case of sintering, maps can be drawn that show the predominant mechanisms for densification under various conditions of pressure and temperature (*e.g.*, References 32, 33, 35, and 36). It can be assumed the densification can be characterized by the deformation of an "average" particle due to the forces transmitted through its interparticle contacts.[35] Hence, constitutive equations can be obtained for the densification rate due to various mechanisms. This then allows the construction of the maps. The analysis depends

Table V. Symbols Used in Table IV[38]

Symbol	Description
A	constant in creep equation
D	relative density
D_c	relative density at which pores close
D_0	initial relative density
D_y	relative density due to yield
D_v	lattice diffusion coefficient
δD_b	boundary thickness x boundary diffusion coefficient
G	grain size
P	external pressure
P_0	Outgassing pressure
P_{1eff}, P_{2eff}	effective pressure on a neck during stage 1 or 2
R	particle radius
T	absolute temperature
Ω	molecular volume
γ_{sv}	specific surface energy
σ_y	yield stress
k_B	Boltzmann's constant
n, n_a, n_b, n_c	creep exponent

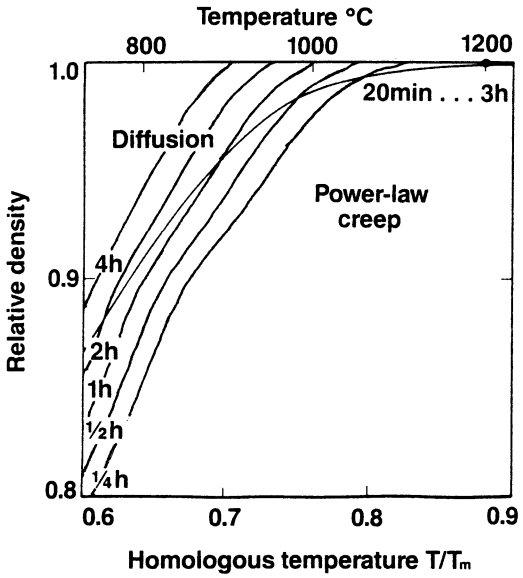

Fig. 12—Densification map for a superalloy powder (high chromium nichrome) showing relative density as a function of homologous temperature T/T_m for a constant pressure of 100 MPa and particle diameter of 50 μm.[35]

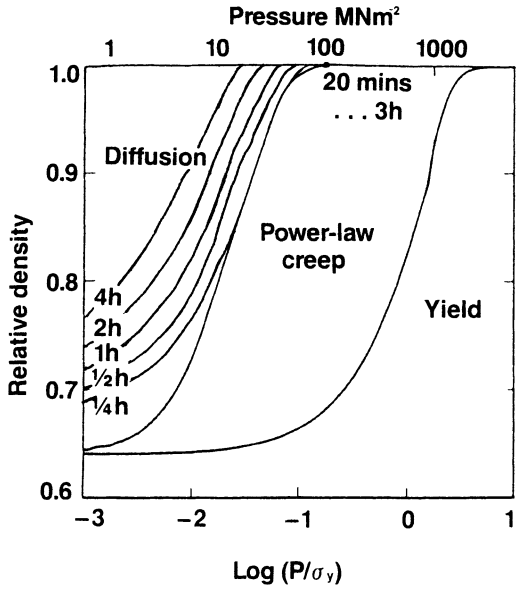

Fig. 13—Densification map for a superalloy powder (high chromium nichrome) showing relative density *vs* normalized pressure P/σ_y for a constant temperature of 1473 K and particle diameter of 50 μm (σ_y is the yield stress).[35]

on the assumption that densification is not a particle rearrangement process. This is thought to be valid, provided the particles are sufficiently close-packed initially. This assumption will be returned to in Section IV–C.

There are three variables—pressure, temperature, and relative density—and, therefore, three kinds of map. These are shown for a densifying superalloy powder in Figures 12 through 14. In Figure 13, for instance, interparticle hole closure for less-dense material under the highest pressures occurs by yield involving dislocation glide. This state is completed suddenly because of the nearly instantaneous operation of this mechanism. The material then enters the

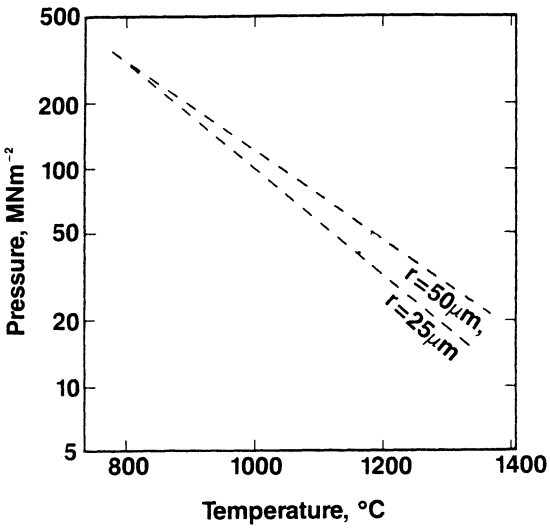

Fig. 14—Densification map showing the combination of pressure P and temperature T required to obtain 99 pct theoretical density in 1 h for two superalloy powders (high chromium nichrome) with different particle radii (50 and 25 μm).[35]

state where hole closure relies on the time-dependent process of power-law creep, where the flow rate is dependent on some exponent of the applied pressure. The exponent is controlled by the material and the processing conditions. It can be as low as 3 or as high as 15. This highlights the value of reaching high pressures in the hipping process. In the final stages, as higher densities are approached, holes are filled by diffusion. The variation in consolidation rate with the external pressure is then approximately linear. In this stage, it is important that pores should be located on grain boundaries for relatively fast diffusion. Thus, the particle size is an important parameter. The smaller the particle size, the lower the compacting pressure required to produce a given density and the faster the densification rate in hipping.

Experiments give agreement with the calculated hipping diagrams when the material parameters are sufficiently well known (*e.g.*, for tool steels, refer to Reference 35). However, the material parameters are often not known. A simple experimental method has been suggested,[39] which involves measurement of the deformation of a single sphere as a direct method of predicting hipping behavior at lower densities (up to ~0.93 relative to the theoretical density). In the same study, it has also been found that hipping defects are associated with deviations from the ideal random dense packing and with differential deformation of particles.[39]

The microscopic approach unites the material properties and processing parameters into an analytical-rate equation; it is, therefore, relatively easy to estimate their roles in the hipping process and the effect on hipped products. Since the microscopic approach describes the densification and deformation behavior by analyzing the microdensification mechanisms, it is physical, rational, and can be conveniently modified to take account of new densification mechanisms. However, it does not relate strain and strain rate to density and densification rate. This makes it difficult to predict shape change, particularly when the stresses contain a deviatoric component.[31]

Various workers have extended the microscopic approach

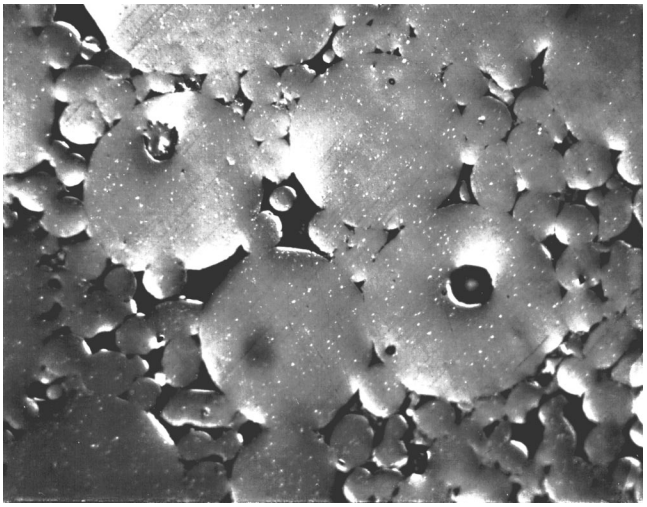

Fig. 15—Micrograph of a hipped sample in the early stages of consolidation. Small particles tend to be heavily deformed. Some internal porosity in the powder is also evident (lighter "interparticle" phase is a remnant of an epoxy added during metallographic preparation). Powder is a bimodally sized, spherical 316L stainless steel, with a nominal 4:1 size ratio and 50 vol pct small particles and is hipped at 840 °C 44 MPa with zero hold time at temperature.[42] Courtesy Dr. Li and Professor Funkenbusch.

to deal with deviations from the assumptions given previously, *i.e.*, (1) ranges of particle sizes; (2) nonspherical particles; (3) densification of castings rather than powders; (4) non-steady-state pressure and temperature; (5) anisotropic shrinkage; and (6) composite materials. Each of these will be dealt with in turn.

1. *Ranges of particle sizes*

Nair and Tien[40] were the first to explicitly incorporate a particle-size mixture into the calculation of hot isostatic press mapping and densification rates and found that there is a separate boundary for each particle size. The array of particle centers is described by a radial distribution function. However, the assumption of equal contact forces on all interparticle contacts led to anomalous results.[41] A simple scheme was then developed[42] for estimating radial distribution functions, which has made modeling of systems with varying particle sizes practical. By distributing the interparticle contact forces to produce uniform contraction around all particles, it has been possible to maintain consistent particle/contact sizes and geometries. Bimodal or continuous size distributions are hipped to a higher density and show large differences in densification rate as a function of density when compared to "monosize" powders. This is mostly due to initial packing-density differences. Smaller particles deform more than larger ones in a mixture leading to, for example, preferential recrystallization of small particles. Preferential deformation of small particles is clear in Figure 15 (taken from Reference 42).

2. *Nonspherical particles*

Lograsso and co-workers have investigated the hipping of angular[43] and irregular[44] powders. Angular titanium powder densified in a similar manner to spherical powder, despite the low initial powder-packing density. The analysis of Arzt *et al.*[35] provided a good basis for predicting the behavior over the range of conditions tested.[43] With irregular copper and yttria powders, the experimental densification rates were found to be higher than those predicted by Arzt *et al.* Lograsso and Lograsso[44] developed empirical relationships incorporating the morphological characteristics into the description of the effective pressure on the particle contacts. Close agreement between experiment and theory was then found.

According to Davies and Jones,[38] when the powder particles are nonspherical, deviations from the standard theory will be largest during the initial stages of densification. For example, if the initial particles are cylinders rather than spheres, an initial packing density can be estimated using the result for the dense random packing of spheres and by taking a mean of the two limiting cases of cylinders in spheres and spheres in cylinders. This gives a packing density of 0.64. A poor estimate of the initial packing density is, in any case, not serious, as an underestimate of the packing density will increase the predicted plastic deformation and initial creep rate, and *vice versa*, so the modeling (by the use of the model of Ashby and co-workers[33,34,35]) is largely self-correcting. Similarly, although the density achieved due to the yield of cylinders may differ slightly from that achieved with spheres, this will not significantly affect the predictions from the model, other than at the start of the densification process. Comparison of the experimental results and the theory gives adequate agreement.[38]

3. *Densification of castings rather than powders*

Pores present in castings tend to be much coarser and with a geometry different from those in compacted powders. It is, therefore, not clear whether models developed for powders can be successfully applied to castings. Artificial specimens with large central holes can be used to mimic the behavior of large casting defects.[45] One difficulty in then applying the Ashby computer program[46] for producing maps is that the program requires a powder-particle size. For castings, the equivalent parameter might then be the average distance between pores. Interestingly, the large pores were essentially eradicated by macroscopic plastic flow during the initial application of pressure and not during the subsequent isothermal part of the hipping cycle. Large artificial pores in ceramics (analogous to the large pores in castings) were found to collapse by grain-boundary sliding.[47]

4. *Non-steady-state pressure and temperature*

Hot isostatic pressing models have usually supposed isothermal conditions and instantaneous pressurization, leading to a well-defined initial density that is taken as the starting point for densification by time-dependent mechanisms. In practice, in the industrial process, heating precedes pressurization, and the gradual increase in pressure at high temperature leads to yield occurring simultaneously with densification by creep and diffusional mechanisms. The contribution to densification of yield and creep in both pure and dispersion-hardened camphene have been determined,[48] and, hence, a revised microscopic hot isostatic pressing model was proposed to take account of the ongoing densification by yield.

5. *Anisotropic shrinkage*

Temperature gradients can cause the so-called "densification wave."[2,49] Such temperature gradients occur particularly when pressure is applied to a sample first, followed by temperature. As heat diffuses into the powder, the hotter surface layer densifies faster than the interior, giving a dense

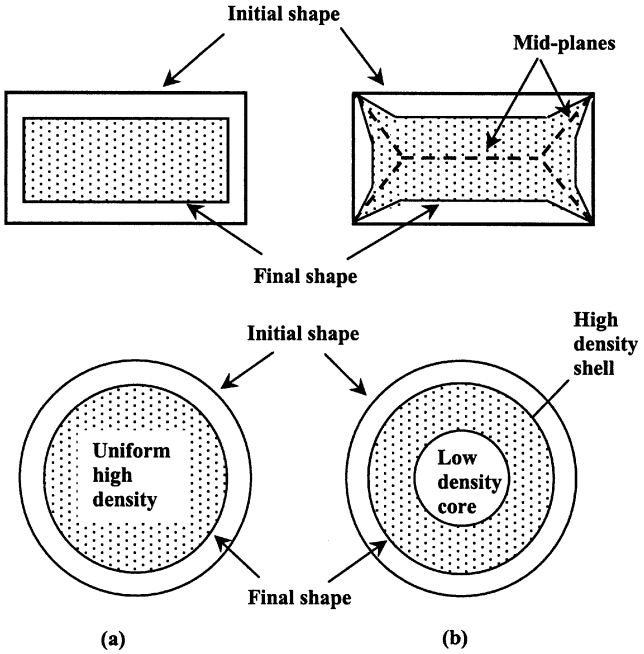

Fig. 16—(*a*) When densification is uniform, the final shape is the same as that of the preform. (*b*) When a densification front forms, shape change, density gradients with residual porosity, and internal stresses result.[2]

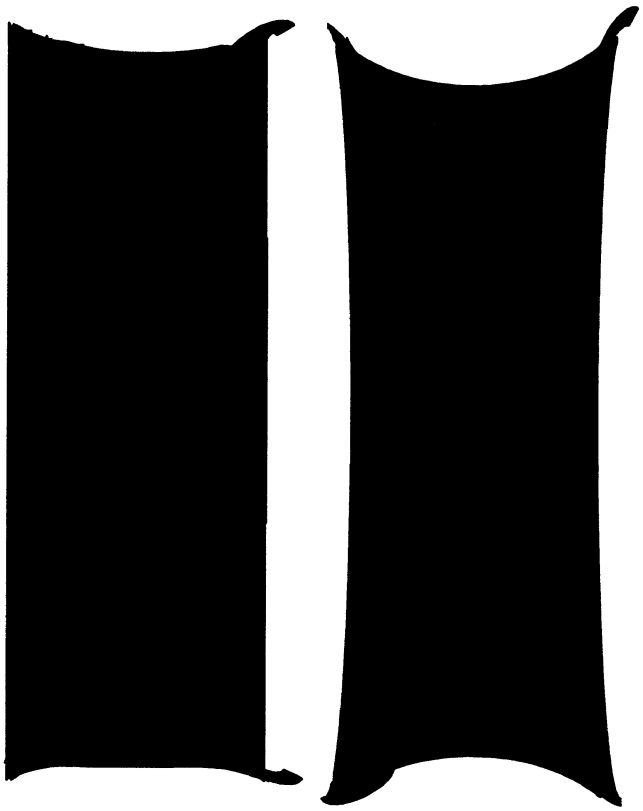

Fig. 17—The densification of tool steel samples. The left sample was heated before it was pressed, so that the temperature was uniform during hipping, giving almost no shape distortion. The right-hand sample was heat treated and pressed at the same time, giving temperature gradients and severe shape change.[2]

skin (Figure 16). The dense skin then supports the load, particularly at the corners. In the extreme case, the inward displacement of the surface is proportional to its distance from the midplanes (the set of planes that are equidistant from all surfaces) of the sample. The shape of the rectangular bar then turns into that of a dog bone as densification proceeds (Figure 17). Heat is conducted through the denser skin faster than through the less-dense interior, further adding to the temperature difference between the surface and the interior. In effect, a densification wave is developing and propagating inward, giving a large shape change. In addition, the dense shell can subsequently impede the shrinkage of the internal part of the billet and contribute to the residual stresses.

6. *Hipping of composites*

The role of a reinforcing phase in a composite (it can be in the form of particles or of fibers) is to constrain the deformation of the surrounding matrix, making it stronger and more creep resistant. However, it is just as effective in constraining the displacements that lead to densification, so that sintering mechanisms, for example, are restrained.[50] Hipping may help to overcome the constraining forces.

Uniaxial consolidation at room temperature of two deformable metal powders (1100 Al and Pb-5 pct Sb) containing various amounts of spherical steel inclusions illustrate that the inclusion phase offers little constraint to matrix deformation at $V_f < 0.20$, but rapidly increasing constraint at larger V_f values.[51] There are two constraining mechanisms. First, the matrix must be deformed more within the composite, because of the excluded volume associated with the packing of particles and inclusions of different sizes. Second, the inclusions form a continuously touching network (predicted by the site-percolation theory and direct observation of deformation flats on steel spheres) that supports a portion of the applied stress and, thus, partially "shields" the deformable phase from the total applied consolidation pressure. These results are reinforced by those for hipping of composite powders.[42,52] The partitioning of deformation between the soft matrix and harder inclusions leads to increased deformation of the softer material.

As far as continuous-fiber metal matrix composites (MMCs) are concerned, the case of hipping of a unidirectional continuous fiber–reinforced composite has been treated from a microscopic point of view,[53] based on the approach of Wilkinson[32] and Ashby and co-workers[35,36] for the simpler problem of hipping of spherical powders. The complex problem is broken down into six, much simpler, subproblems, and the contributions to densification are summed. Densification maps can then be produced.

The local residual stresses in a unidirectional fiber–reinforced MMC made of an elastic fiber and a thermoviscoplastic matrix have been predicted using an axisymmetric micromechanical model.[54] Slow cooling rates from the hipping temperature under sustained hydrostatic pressure give reduced residual stresses because of inelastic deformation of the matrix along the cooling path. These theoretical predictions do not appear to have been experimentally tested as yet.

In the development of the microscopic approach, micromechanical models for densification have been combined with empirical kinetic relationships for both grain size and interfacial reaction-layer thickness during the hipping of

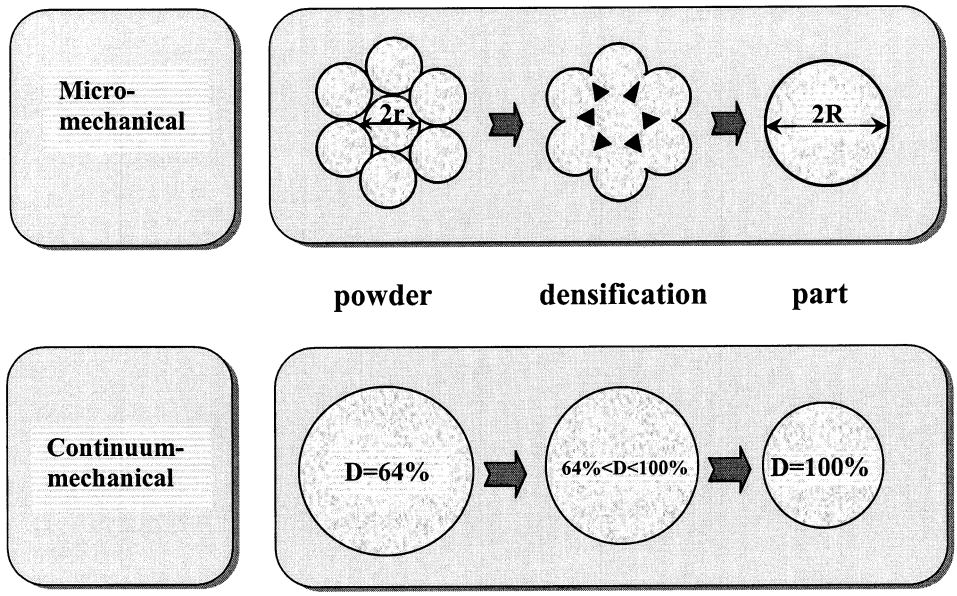

Fig. 18—Schematic demonstration of the basic methods for numerical modeling of powder particles. *D*: relative density; *r*: characteristic particle size; and *R* characteristic size of part.[56]

physical Vapor deposition (PVD)–coated Ti-matrix composite fibers.[55] The relative density was very sensitive to the small grain size of the PVD matrix. For the system investigated (Ti-6Al-4V-coated SiC monofilaments), diffusion-accommodated grain sliding was considered to be the dominant densification mechanism. Again, experimental testing of these predictions has not yet been reported.

The creep of metal-like organic compounds such as succinonitrile and camphene, which contain a dispersed phase of fine hard alumina particles, has been investigated to find the effects of the reinforcement on densification.[38] The hard particles generate a friction stress, and this can be incorporated into the set of densification equations. There are some discrepancies between the predictions and the experimental results. As the relative density increases, the effective pressure decreases from extremely high values at the onset of densification to the applied isostatic pressure in the limit of full densification. The effective pressure gives rise to an effective stress, causing densification, which, therefore, also decreases with increasing relative density. The discrepancies may be due to the way in which the relevant creep equations include this effective stress.

B. *Macroscropic Models*

1. *General comments*

In contrast to the microscopic approach, the macroscopic approach treats the powder compact as a continuous medium.[31] Figure 18 illustrates the difference.[56] Constitutive equations describing the macroscale deformation of porous materials are obtained by modification of plastic theory for solid materials.[57–65] These do not take into account particle rearrangements and interparticle sliding and rely on the assumption that the particles are initially densely packed. Solving the equations gives the density distribution and final shape of the component. A yield function has been proposed for a porous material at room temperature.[60] This was extended to high temperatures using a viscoplastic model of power-law creep.[66] The deformation and stress distribution in a powder compact under hipping could then be studied using finite-element analysis.[62] The finite-element modeling of powder consolidation has recently been reviewed.[67] Such simulations operate by examining the behavior of a computer-generated array of particles or "nodes" using finite elements and depend on having an adequately sized array to characterize the real macroscopic system. It should be noted that the use of finite-element modeling is not restricted to the macroscopic approach; it can be combined with the microscopic understanding.

In the macroscopic approach, *i.e.*, a continuum mechanical model, the general plasticity theory for solids is modified for a porous continuum, and a constitutive equation is constructed that relates the strain increment to the stresses. In the equation, there are some important coefficients that have to be determined experimentally. The values of these coefficients obtained under certain experimental conditions may not be extrapolated to other conditions. The reason for this is that, according to hipping theory,[35,36] the densification rate is controlled mainly by a rate-governing mechanism that depends on the density and hipping conditions. For example, values of the coefficients obtained under high pressure and low temperature, where power-law creep is the governing mechanism, may not be applicable in conditions of low pressure and high temperature, where diffusion mechanisms usually control densification. This feature makes the macroscopic approach empirical and difficult to combine with a new densification mechanism. However, the continuum mechanical model can predict the shape change caused by hipping and is convenient to use for a powder component with a complex geometry, because it has a more concise formulation and fewer parameters are involved than in the microscopic approach.

As an example of what can be achieved, quite-accurate

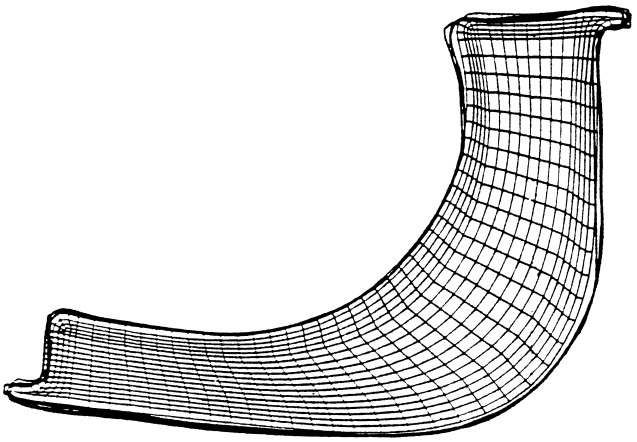

Fig. 19—Predicted deformed geometry contrasted against three sets of actual measurements of pressed parts.[68]

results (Figure 19) have been obtained[68,69,70] with finite-element modeling, using the macroscopic approach with the governing equation for the macroscopic viscoplastic potential (Φ) of a porous powder compact acting as a compressible, continuous medium:

$$\Phi = S^2 + b(\beta)p^2 - c(\beta)s^2$$

Here, S is the magnitude of the deviatoric stress tensor, β is the relative density, p is the pressure as a function of the Cauchy stress tensor, and the deviatoric stress(s) of the powder is $\sqrt{2/3}\overline{\sigma}$, where $\overline{\sigma}$ is the tensile yield stress. The functions $b(\beta)$ and $c(\beta)$ are determined experimentally for each material. Elasto-plastic and compressible viscoplastic models are used for the container and powder materials, respectively. The thermal and density dependence of the mechanical and thermal properties of the powder are taken into account. Figure 19 represents the result after one iteration. Starting with an experience-based container design, the container geometry is successively refined based on the difference between the target geometry and that predicted by the modeling. For axisymmetric components, three to four iterations are typically enough to converge to a successful design.

Finite-element models have been reviewed[71] for hipping. The normal modeling procedure includes the definition of constitutive equations, either from experimental data or from microstructure-based models, and the integration of these equations in a finite-element code, which allows the simulation of the consolidation. In some articles, comparison of the results with a real component is sometimes given, but the validation may be rather incomplete. The comparison of models is also rather difficult, since constitutive equations may have various mathematical formulations and be based on different experimental results. Furthermore, numerical integration techniques vary from one code to another.

Benchmarking to compare models is, thus, important. A major international research program was initiated in 1994 to carry this out for hipping,[71–83] and the results were reported in 1997[84] and in further articles (*e.g.*, References 85 and 86). The groups involved are shown in Tables VI and VII. To obtain the material parameters, two methods have been proposed. One is based on the continuous measurement of a characteristic dimension of the cylindrical specimen,[74,87] for example, by using an *in-situ* dilatometer (Figure 20). The density variation can then be estimated based on hypotheses about the sample geometry and can thickness. Alternatively, interrupted hipping tests can be carried out and the density measured after each test.[88] The difficulty with this is that the densification cannot be stopped suddenly and is still active during the temperature and pressure unload. The most convenient experiment to study the behavior of the material under deviatoric stress is a simple compression test, *i.e.*, uniaxial compression with no lateral pressure. Constant-displacement-rate tests can be carried out on specimens of different densities, and the stationary stress is obtained as a function of strain rate and density.[77] Die compression tests cannot be directly interpreted, because the lateral pressure is generally unknown.[62] Triaxial pressing may be used, as it allows independent axial and radial pressing.[75] However, accurate strain measurement may be difficult in such systems.[69]

The report of the 1997 workshop on the benchmarking study[84] does not give a summary comparison of the results of the different finite-element method (FEM) simulations. The key articles are References 89 through 94, but the results are not given in such a form that, for example, one diagram of final shape can be placed over another to compare the quality of the fit. There is a comparison of two different modeling approaches in Reference 94. However, what is clear is that good agreement between numerical simulation and experiment can be obtained. For example, the results of Reference 93, obtained using a three-dimensional simulation for a three-dimensional part, are shown in Table VIII. Figure 21 shows all the dimensions measured in the validation work. The table shows the initial values for three representative dimensions (A, B, and I), their final measured values, and the final simulated values. For a 160 mm original dimension (A), the simulation is 143.027 mm, in comparison with the measured final dimension of 143.561 mm, giving agreement to within 1 mm on this length scale. The model used Abouaf's viscoplastic equation.[62] Various articles in the workshop proceedings propose refinements to this, including Reference 91, where, above 700 °C, it is proposed that the inelastic strain rate must be decomposed into a viscoplastic part, represented by Abouaf's equation, and a nontime-dependent plastic part. If Abouaf's viscoplastic model is used alone, the experimental densification is underestimated. Sanchez *et al.*[92] also suggest that the rheological functions for use in Abouaf's equation must be determined by an iterative procedure. This arises because the rheological functions are usually determined by assuming that the mean pressure in the sample is homogeneous and equal to the applied pressure. However, numerical modeling shows this assumption to be false. The applied pressure is not fully transmitted to the powder, because of the container stiffness.

Good agreement (to within 1 pct) between the FEM simulation and a hipped component with a core has been obtained by Svoboda *et al.*,[82,85,86] as shown in Figure 22.

There has been recent work on bringing together the macro and micro approaches,[31] essentially introducing the rate equations of densification into the microscopic constitutive equation. The resulting equation in Reference 31 is potentially as important as Hooke's law for elasticity and the Prandtl–Reuss equation for plasticity. It can, in principle,

Table VI. List and Activity of the Teams Participating in Experimental Testing for International Benchmarking Study of Hot Isostatic Press Modeling[71]

Organization	Country	Team Leaders	Tests	Reference
CEREM, Grenoble	France	Dellis and Bouaziz	iHIP	72
Crucible Research	US	Eisen	DHIP	68
University of Pohang	Korea	Kim	iHIP, HF, and HP	73
Ecole des Mines, D'Albi	France	Levaillant	HF	
University of Karlsruhe	Germany	Oberacker	DHIP	74
Carnegie-Mellon University	US	Piehler	HTP	75
LNT, Moscow	Russia	Samarov and Seliverstov	iHIP and HF	76
Laboratoire 3S, Grenoble	France	Bouaziz, Stutz, and Ouedraogo	HF	77
University of Lulea	Sweden	Svoboda and Haggblad	DHIP	78

Abbreviations: iHIP—interrupted hot isostatic pressing; dHIP—hot isostatic pressing with *in-situ* dilatometric measurement; HF—hot forging; HP—hot pressing; and HTP—hot triaxial pressing.

Table VII. List of the Teams Participating in the International Benchmarking Study of Finite Element Simulation of Hipping[71]

Organization	Country	Responsible Worker	Tests	Reference
University of Pennsylvania	US	Aravas	Abaqus	*
Indian Institute of Technology, Kanpur	India	Bhargava	hdc	*
Bulgarian Academy of Sciences, Sofia	Bulgaria	Bontcheva	hdc	*
CEREM, Grenoble	France	Bouaziz, Dellis	PreCAD	72
Ohio State University	USA	Jinka	Allform	79
IFAM, Bremen	Germany	Khazami-Zadeh	Abaqus	80
University of Pohang	Korea	Kim	Abaqus	73
Defence Metals Research Laboratory, Kanchanbagh	India	Ramakhrishnam	hdc	*
LNT	Russia	Samarov, Seliverstov	hdc	76
Institute of Problems in Materials Science	Ukraine	Shtern	hdc	81
University of Lulea	Sweden	Svoboda, Haggblad	Nike2D	82
MATSYS, Arlington	US	Zarah	Prosim	83

Abbreviations: hdc home developed code.
*No reference for published work on Hipping available.

be used for isostatic or nonisostatic loads. A numerical method is necessary for solving the equation, because of its complexity. Results of applying the equation are due to be published soon.

2. *Anisotropic shrinkage*

Three factors have an impact on the shape of the final article:[95]

(1) temperature gradients,
(2) inhomogeneity in the body being hipped, *e.g.*, density gradients, and
(3) the load-bearing capacity of the container wall and welds.

These all introduce a deviatoric stress, even though the load applied during the hipping cycle is hydrostatic. Indeed, it has been argued that a small deviatoric stress superposed on a relatively large hydrostatic load can significantly increase the predicted densification rates.[96]

As mentioned earlier, temperature gradients can cause a densification wave.[97] The ratio between the velocity of the temperature front and that of the density front has been determined,[49] and the dependence of the densification-wave effect on the nonlinearity of the rheological properties of the matrix-phase materials was analyzed using a macroscopic approach.[98] It was shown that the densification wave appears under high degrees of nonlinearity only. The densification wave might be avoided by nonuniform heating of the billet, but there are considerable practical difficulties in achieving this. The FEM under isothermal and nonisothermal conditions has shown that the latter leads to a nonisostatic pressure.[99]

For inhomogeneity in the body being hipped, *e.g.*, density gradients, billets could be prepared with inhomogeneously distributed porosity[100] to combat the resulting shape change. However, again, there are significant practical difficulties.

The influence of the container is most important in determining the final shape of the article.[101] The shrinkage anisotropy is accompanied by the appearance of the deviatoric stress component in the porous volume. This problem has been studied for pressing of a powder cylinder in a long tube, without considering the influence of the container bottoms.[102] The deformation of the container has also been analyzed on the basis of shell theory.[103,104] It was demonstrated that the axial shrinkage of a powder is always smaller than the radial shrinkage,[103] as observed experimentally for alumina powder[87,105] and for copper,[101] provided that thermo-elastic effects can be neglected. This is essentially due to the fact that the can supports a larger load in the axial direction, compared to the radial direction, during plastic deformation.[104]

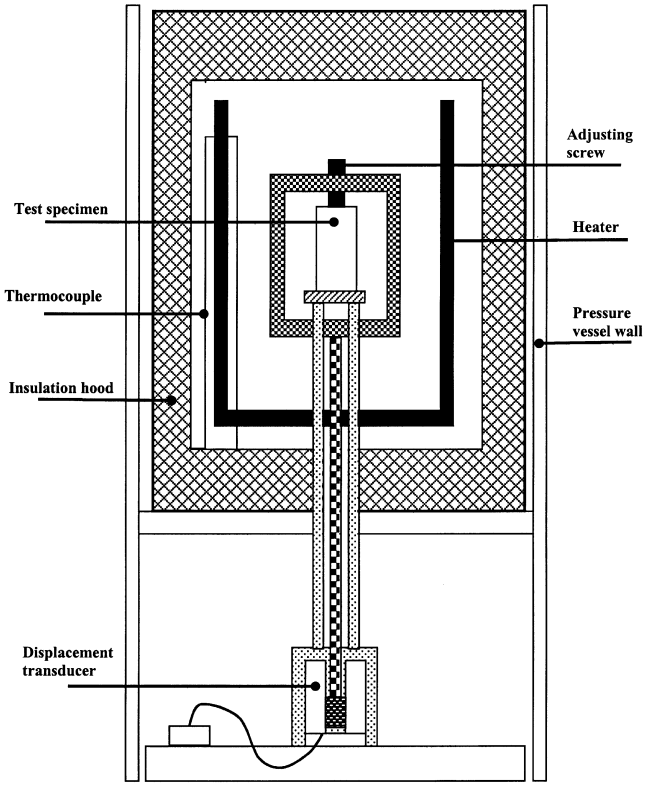

Fig. 20—Scheme of an *in-situ* hot isostatic press dilatometer.[74]

Table VIII. Initial Values, Final Measured Values after Hipping, and Simulated Values after Hipping for Representative Dimensions A, B, and I on the Three-Dimensional Part in Figure 21[93]

Dimension	Initial Value (mm)	Measured Final Value (mm)	Simulated Final Value (mm)
A	160.807	143.561	143.027
B	230.990	206.324	205.232
I	76.987	68.250	66.626

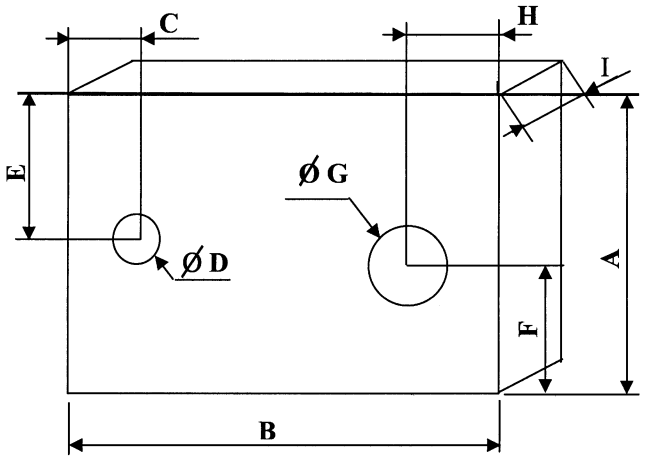

Fig. 21—Three-dimensional part for validation of simulation in comparison with measured final dimensions after hipping.[89] The letters A . . . I represent dimensions of the part measured in the validation. Table VIII gives the initial values for representative dimensions A, B, and I, the measured final values, and the simulated final values. D and G are on through holes.

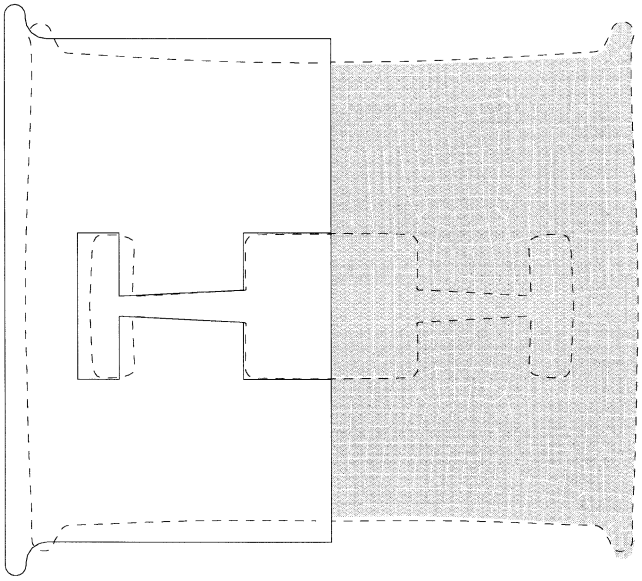

Fig. 22—Comparison between initial undeformed geometry (left side of the figure), resulting geometry from the simulation (right side), and that from the inspection. The result of the simulation is shown by FEM mesh. Bold lines show the initial shape of the container and the core; dashed lines show the result from the inspection obtained using CMM.[85]

The behavior of the container and its interaction with the powder/component must be an inherent part of the development of modeling. Several of the articles identified in Table VII include such considerations. For hot deformation processes, the nonlinearity of the viscous-plastic properties of not just the powder, but also the container, should be taken into account. The FEM provides the fullest analysis of the deformation of the powder-container system.[106–111] A modification of the variational principle for determining the field of unknown kinematic parameters (velocities and displacements) has been suggested, along with the idea of using different wall thicknesses for the lateral and end walls in order to control the shrinkage anisotropy.[95,111] The ratio between the container-wall thicknesses should be proportional to the ratio of the dimensions of the internal space of the container in the directions perpendicular to the walls. Other workers are also developing FEM simulations.

Good agreement is claimed (although no actual dimensions are supplied, so it is difficult to compare the results with other workers) between experimental data for hipping of alumina-powder compacts and FEM calculations,[112] using the constitutive equations for grain growth and diffusional creep from References 113 and 114 and those for power-law creep from References 115 and 116. Kuhn and McMeeking[115] suggested a constitutive model to analyze the creep behavior of metal-powder compacts, which have relatively low densities ($D < 0.9$) under general loading, by approximating the contact deformation of metal-powder particles. Sofronis and McMeeking[116] dealt with the higher densities ($D > 0.9$) under general loading by finite-element analysis for a hollow sphere. If the alumina powder is encapsulated, the container causes nonuniform densification and shape change, but has little effect on the densification rate.

Similar work has been carried out for copper powder.[117] The agreement is reasonable for density predictions (although, again, no shape predictions are given), provided that the stress

is hydrostatic, but not if deviatoric stresses increase. A possible explanation for the disagreement may be the irregular size and shape of the copper-powder particles. The theory is based on monosized spherical powder particles.

3. *Macroscopic approach for composites*

The FEM predictions have been compared with experiments for foil-fiber-foil and tape-cast monotapes.[118,119] For foil-fiber-foil layups, there is an important influence on the consolidation time of interface friction–shear factors, and the consolidation time is sensitive to small variations in hipping temperature and material flow properties such as strain-rate sensitivity. These factors were less important for the tape-cast monotape layups.

For modeling, there are two issues for consideration in the deformation behavior of fibre-reinforced MMCs:

(1) anisotropic mechanical (in particular, viscous) properties, and
(2) large imperfections (large-scale pores), which influence the shrinkage kinetics during hipping.

From a topological point of view, these imperfections (for example, those arising for the MMC if a fiber is missing from the array) cause "heterogeneity of the void phase," *i.e.*, the porous structure becomes bimodal. Pores of different scales have different shrinkage intensities and can hinder the densification of each other.[40,41] The problem has been taken further using the continuum theory of sintering as a theoretical basis.[120,121]

IV. OTHER RECENT DEVELOPMENTS

A. *Modeling of the Effects of Hipping on Microstructure*

A method has recently been developed[122] to model the dynamic behavior of powder metallurgy (PM) superalloys during hot isostatic pressing. The power-dissipative efficiency during the hipping process was related to the relative density and the strain-rate sensitivity index. The research workers carried out isothermal constant-strain-rate tests and, hence, predicted the microstructural evolution of the PM Rene 95 alloy during hipping. The results suggest that hipping in the temperature range from 1100 °C to 1120 °C and a strain-rate range of $l0^{-4}$ to 10^{-3} s^{-1} may eliminate residual dendrites and ensure consistent microstructures and properties, in good agreement with practical experience.

This is an area that warrants further attention, because the microstructure is critical to the properties of the hipped product. The microstructure (*e.g.*, grain size and existence of prior particle boundaries) cannot be predicted from the macroscopic approach.

B. *In-Situ Sensors*

The use of *in-situ* dilatometers for continuous measurement of dimensions during hipping has already been mentioned (Figure 20 of Reference 74 and Section III–B–1). Proposed systems rely on measuring the vertical displacement.[74,123] In contrast, eddy-current sensors are generally arranged to detect a change in diameter.[101,124,126] They operate on a two-coil technique, in which a primary coil induces a uniform electromagnetic field of variable frequency and a secondary coil senses the perturbation to this field by the sample. At high frequencies, because of the skin effect, the perturbations to the field are controlled only by the geometry of the component and not by its electrical conductivity. Hence, it is possible to measure a component's dimensions.

The development of such *in-situ* sensors has provided a means for evaluating models (*e.g.*, Reference 101). The difficulty with dilatometers and eddy-current sensors is that interpreting the signal to obtain information on densification relies on the sample having a simple geometry.

Stubbs and Dutton[127] have recently developed an ultrasonic sensor that is capable of emitting and receiving ultrasonic energy at >900 °C and >150 MPa and can measure workpiece deformation during hipping. A reliable sensor that could provide information on the actual consolidation of the material would save hipping time and cost. Further, hipping runs could be terminated as soon as consolidation is complete, reducing undesired effects due to holding the materials at elevated temperatures for extended periods of time.

C. *Importance of Densification during the Initial Transient*

In several earlier sections (*e.g.*, sections III–A–3 and 4), the importance of the initial transient conditions as the hipping pressure and temperature are approached was identified. This is further emphasised by recent experimental work,[128] showing that a major proportion of the densification of hipped Ti-6Al-4V powders occurs in the transient period. This is due to particle translation and rotation. In Reference 128, it was shown that smaller particles deform substantially more than larger neighboring particles, and this deformation contributes to the continued shifting motion of large particles. In addition, porosity in the samples is always cusped, never spherical or cylindrical, in contrast to the assumptions in most FEM simulations. It was concluded that the microscopic models do not accurately describe the interparticle geometry in stage 2 and so do not accommodate the observed particle movement in early stages. The observed behavior is only partially addressed by static continuum (macroscopic) models and is not adequately addressed by static and dynamic continuum models, which do not incoporate granular flow behavior. Despite these comments, however, there has been a degree of success in modeling shape change with both microscopic and macroscopic approaches.

D. *Reactive Hipping*

When the synthesis of a compound occurs during heating to a hipping temperature, this is termed reactive hipping (*e.g.*, Reference 129). For example,[4] TiB_2 can be formed from a mixture of Ti and B powders encapsulated and heated in a hot isostatic press to 700 °C, under a pressure of 100 MPa. The exothermic reaction is then ignited using a heated wire implanted in the compact. Rapid self-heating occurs, and the compact densifies under the combined action of its own heat and the external pressure. Fine-grained products can result. Various compounds have been produced in this way, including $NbAl_3$, Nb_3Sn, FeAl, Ni_3Al, $MoSi_2$-SiC, TiAl, and Al_20_3-TiC.

As yet there, has been no attempt to apply hot isostatic press FEM modeling to reactive hipping. Reactive hipping could lead to the processing of materials and composites that will greatly expand the use of hipping.

V. CONCLUDING REMARKS

The basic science of hipping has been summarized. Models of hipping have been explored, differentiating between microscopic and macroscopic approaches. The effects of having a range of particle sizes rather than monosized particles and having nonspherical particles have been discussed. The densification of castings, rather than powders, and the effects of non-steady-state pressure and temperature have been described. Particular emphasis has been given to anisotropic shrinkage, as this is a major issue for industrial practitioners. The application of hipping to MMCs, and models thereof, has also been included.

There has been an explosion in modeling activity in the 1990s, to some extent supported by experimental data and developments (*e.g.*, the use of *in-situ* sensors to monitor shape change and densification). However, the technology is constantly evolving with, for example, innovations in rapid cooling and reactive hipping and with little attempt as yet to take these into account in the models. In addition, questions have recently been raised about the major role that particle rearrangement during the initial transient may play in densification. Further, for those applications requiring containment, there is a need to identify which models allow the container dimensions and material specifications to be most reliably identified. What is clear is that hipping is a far more "dynamic" process than originally envisaged, with particles shifting around in the initial stages and major plastic flow. In this respect, it is quite distinct from sintering without pressure.

A major area for development is the prediction of the effects of hipping on microstructural features such as grain size and precipitate distributions.

ACKNOWLEDGMENTS

The authors thank Professors H. Jones and G.W. Greenwood for helpful comments on the manuscript, Drs. Jae Kyun Yang, Doh-Yeon Kim, and Sang-Ho Lee for permission to reproduce Figure 10, Professor P.D. Funkenbusch, Dr. E. Li, and the publishers of *Metallurgical and Materials Transactions* for permission to reproduce Figure 15, Drs. Canga, Eisen, and Trasorras, MPIF (Princeton, NJ), for permission to reproduce Figure 19, Drs. Svoboda, Haggblad, and Karlsson for permission to reproduce Figure 22 and Dr. Bouvard for kindly supplying a copy of the *Proceedings of the '97 Workshop*.[84]

REFERENCES

1. G.W. Greenwood: *Proc 17th Annual BICTA Conf.*, Stratford-Upon-Avon, Sept. 1983, British Investment Casters Trade Association, Alvechurch, 1983, pp. 11:1-11:8.
2. M.F. Ashby: *Proc. Int. Conf. on Hot Isostatic Pressing*, Lulea, June 15–17, 1987, T. Garvare, ed., Centek, Lulea, Sweden, 1987, pp. 29-40.
3. H.V. Atkinson and B.A. Rickinson: *Hot Isostatic Processing*, Adam Hilger, Bristol, 1991, p. 190.
4. R.M. German: *Sintering Theory and Practice*, Wiley, New York, NY, 1996,
5. H.A. Saller, S.J. Paprocki, R.W. Dayton, and E.S. Hodge: U.S. Patent 687,842 and Canadian Patent 680,160, 1964.
6. E. Lardner: *Metallurgist Mater. Technologist*, 1982, vol. 14 (3), pp. 115-18.
7. T. Crousatier: *Fonderie*, 1975, vol. 347, pp. 265-80.
8. G.E. Wasielewski and N.R. Lindblad: *Proc 2nd Int. Conf. Superalloys Processing*, TMS-AIME, Champion, PA, 1972, pp. D-l-D-24.
9. Battelle MCIC Report No. MCIC-77-34, Columbus Laboratories, Battelle, Columbus, OH, 1987.
10. M.B. Waldron and B.L. Daniell: *Sintering*, Heyden, London, 1978, p. 62.
11. S. Quaranta and L.B.P. Antona: *Alluminio*, 1981, pp. 96-99.
12. E.A. Olevsky: *Mater. Sci. Eng.* 1998, vol. R23(2), pp. 41-100.
13. J.K. Mackenzie and R. Shuttleworth: *Proc. Phys. Soc.*, 1949, vol. 62, pp. 833-52.
14. R.L. Coble and M.C. Flemings: *Metall. Trans.*, 1971, vol. 2, pp. 409-15.
15. P. Murray, E.P. Rogers, and A.E. Williams: *Trans. Br. Ceram. Soc.*, 1954, vol. 53, pp. 474-510.
16. G.W. Greenwood: *J. Mater. Sci.*, 1969, vol. 4, pp. 320-22.
17. R.S. Nelson, D.J. Mazey, and R.S. Barnes: *Phil. Mag.*, 1965, vol. 11, pp. 91-111.
18. G.W. Greenwood: *Report of Manchester Symp. on Phase Transformations*, Institute of Metals, London, 1968, pp. 103-10.
19. M.V. Speight and G.W. Greenwood: *Phil. Mag.*, 1964, vol. 9, pp. 683-89.
20. R.L. Coble: *J Appl. Phys.*, 1970, vol. 41, pp. 4798-4807.
21. F.W. Crossman and M.F. Ashby: *Acta Metall.*, 1975, vol 23, pp. 425-40.
22. D.S. Wilkinson and M.F. Ashby: *Acta Metall.*, 1975, vol. 23, pp. 1277-85.
23. W. Schatt, E. Friedrich, and E.P. Wieters: *Rev. Powder Met. Phys. Ceram.*, 1986, vol. 3, pp. 1-111.
24. B.H. Alexander and R.W. Balluffi: *Acta Metall.*, 1957, vol. 5, pp. 666-77.
25. G.W. Greenwood, H. Jones, and J.H. Woodhead: *Phil. Mag.*, 1975, vol 31, pp. 39-46.
26. M. Basaran, T.Z. Kattamis, R. Mehrabian, and M.C. Flemings: *Metall. Trans.*, 1973, vol. 4, pp. 2429-34.
27. O.H. Kwon and G.L. Messing: *Isostatic Pressing Theory and Applications*, ASM, Metals Park, OH, 1991, pp. 165-70.
28. K.G. Ewsuk and G.L. Messing: *J. Mater. Sci.*, 1984, vol. 19, pp. 1530-34.
29. J.E. Smugeresky: personal communication with R.M. German, Sandia National Laboratory, CA.
30. S.H. Lee, J.K. Yang, and D.Y. Kim: *J. Am. Ceram. Soc.*, 1993, vol. 76 (4), pp. 880-84.
31. W.B. Li and H.A. Haggblad: *Powder Metall.*, 1997, vol. 40, pp. 279-81.
32. D.S. Wilkinson: Ph.D. Thesis, University of Cambridge, Cambridge, United Kingdom, 1977.
33. F.B. Swinkels, D.S. Wilkinson, E. Arzt, and M.F. Ashby: *Acta Metall.*, 1983, vol. 31, pp. 1829-40.
34. E. Arzt: *Acta Metall.*, 1982, vol. 30, pp. 1883-90.
35. E. Arzt, M.F. Ashby, and K.E. Easterling: *Metall. Trans. A*, 1983, vol 14A, pp. 211-21.
36. A.S. Helle, K.E. Easterling, and M.F. Ashby: *Acta Metall.*, 1985, vol. 33, pp. 2163-74.
37. P.S. Gilman and G.H. Gessinger: *Powder. Met. Int.*, 1980, vol. 12, pp. 38-40.
38. G.C. Davies and D.R.H. Jones: *Acta Mater.*, 1997, vol. 45, pp. 775-89.
39. W.A. Kaysser, M. Aslan, E. Arzt, M. Mitkov, and G. Petzow: *Powder Metall.*, 1988, vol. 31, pp. 63-69.
40. S.V.Nair and J.K. Tien: *Metall. Trans. A.*, 1987, vol. 18A, pp. 97-107.
41. E.K.H.Li and P.D. Funkenbusch: *Acta Metall.*, 1989, vol. 37, pp. 1645-55.
42. E.K.H. Li and P.D. Funkenbusch: *Metall. Trans. A*, 1993, vol. 24A, pp 1345-54.
43. B.K. Lograsso and D.A. Koss: *Metall. Trans. A*, 1988, vol. 19A, pp. 1767-73.
44. B.K. Lograsso and T.A. Lograsso: *Mater. Manufacturing Processes*, 1994, vol. 9, pp. 681-94.
45. A.J. Fletcher and S. King: *Mater. Sci. Technol.*, 1996, vol. 12, pp. 477-82.
46. M.F. Ashby: HIP487, version HIP6.1, Cambridge University, Cambridge, United Kingdom, 1990, and accompanying documentation on *Sintering and Isostatic Pressing Diagrams*.
47. K.S. Oh, D.Y. Kim, and S.J. Cho: *J. Am. Ceram. Soc.*, 1995, vol. 78, pp. 2537-40.
48. G.C. Davies and D.R.H. Jones: *Scripta Mater.*, 1997, vol. 37, pp. 1745-51.
49. W.B. Li, M.F. Ashby, and K.E. Easterling: *Acta Metall.*, 1987, vol. 35, pp. 2831-42.

50. M.F. Ashby, S. Bahk, J. Berk, and D. Turnbull: *Progr. Mater. Sci.*, 1980, vol. 25, pp. 1-34.
51. F.F. Lange, L. Atteras, F. Zok, and J.R. Porter: *Acta Metall. Mater.*, 1991, vol. 39, pp. 209-19.
52. E. Pagounis, M. Talvitie, and V.K. Lindroos: *Mater. Res. Bull.*, 1996, vol. 31, pp. 1277-85.
53. H.N.G. Wadley and D.M. Elzey: Proc. Conf. *Composites Design, Manufacture and Application*, ICCM VIII, Section 12-21, S.W. Tsai and G.S. Springer, eds., Honolulu, July 15–19, 1991, Society for Advancement of Materials and Process Engineering (SAMPE), 1991, pp. B1-B11.
54. Y.A. Bahei-el-din and G.J. Dvorak: *Acta Metall. Mater.*, 1995, vol. 43, pp. 2531-39.
55. R. Vancheeswaran, D.M. Elzey, J.M. Kunze, and H.N.G. Wadley: *Mater. Sci. Eng. A*, 1998, vol. 244, pp. 49-57.
56. M. Khazami-Zadeh and F. Petzoldt: *Advances in Powder Metallurgy and Particulate Materials*, Metal Powder Industries Federation (MPIF), Princeton, NJ, 1995, vol. 2, pp. 5-125-5-128.
57. H.A. Kuhn and C.L. Downey: *Int. J. Powder Metall.*, 1971, vol 7, pp. 15-25.
58. R.J. Green: *Int. J. Mech. Sci.*, 1972, vol. 14, pp. 215-24.
59. M. Oyane, S. Shima, and Y. Kono: *Bull. Jpn. Inst. Mech. Eng.*, 1973, vol 16, pp 1254-62.
60. S. Shima and M. Oyane: *Int. J. Mech. Sci.*, 1976, vol. 18, pp. 285-91.
61. M. Abouaf and J.L. Chenot: *J. Mecanique Theorique Appl.*, 1986, vol. 5, pp. 121-40.
62. M. Abouaf, J.L. Chenot, G. Raisson, and P. Bauduin: *Int. J. Num. Methods Eng.*, 1988, vol. 25, pp.191-212.
63. S. Yossifon, Y. Gefen, D. Kalin, and O. Yeheskel: *Hot Isostatic Pressing: Theory and Applications: Proc. 2nd Int. Conf. on HIP*, R.J. Schaefer and M. Linzer, eds., ASM INTERNATIONAL, Materials Park OH, 1991, pp. 63-71.
64. S. Shima: *Hot Isostatic Pressing: Theory and Applications. Proc. 3rd Conf. on HIP*, M. Koizumi, ed., Elsevier Science, Barking, 1992, pp. 11-16.
65. K.I. Mori, K. Oskada, and T. Hirano: *Hot Isostatic Pressing: Theory and Applications: Proc. 3rd Int. Conf. on HIP*, M. Koizumi, ed., Elsevier Science, Barking, 1992, pp. 29-34.
66. A. Nohara, T. Nakagawa, T. Soh, and T. Shinke: *Int. J. Num. Methods Eng.*, 1988, vol. 25, pp. 213-25.
67. N. Ramakrishnan and V.S. Arunachalam: *Progr. Mater. Sci.*, 1997, vol. 42, pp. 253-61.
68. J.R.L. Trasorras, M.E. Canga, and W.B. Eisen: *Advances in Powder Metallurgy and Particulate Materials*, Proc. Conf., C Lall and A.J. Neupaver, eds., Metal Powder Industries Federation (MPIF), Princeton, NJ, 1994, vol.7, pp. 51-69.
69. J.F. Zarzour, J.R.L. Trasorras, J. Xu, and J.J. Conway: *Advances in Powder Metallurgy and Particulate Materials*, M. Phillips and J. Porter, eds., Metal Powder Industries Federation (MPIF), Princeton NJ, 1995, vol. 2, Part 5, pp. 89-112.
70. J.R.L. Trasorras, R. Parameswaran, J. Xu, R. Anbajagane, and V.B.S. Rachakonda: *Advances in Powder Metallurgy and Particulate Materials*, M. Phillips and J. Porter, eds., Powder Industries Federation (MPIF), Princeton, NJ, 1995, vol. 2, Part 5, pp. 139-52
71. D. Bouvard, O. Bouaziz, C. Dellis, and A.G.K. Jinka: *Proc. Int. Conf. on Hot Isostatic Pressing*, Andover, MA, May 20–22, 1996, ASM, Materials Park, OH, 1996, pp. 53-57.
72. O. Bouaziz, R. Baccino, C. Dellis, F. Moret, and P. Stutz: *Proc. Int. Conf. on Hot Isostatic Pressing*, May 20–22, 1996, Andover, MA, ASM, Material Park, OH, 1996, pp. 145-50.
73. Y.S. Kwon and K.T. Kim: *Powder Metallurgy World Congress*, Les Editions de Physique, Les Ulis, 1994, EPMA, Shrewsbury, 1994, vol. I, pp. 779-82.
74. A. Kuhne, R. Oberacker, and T. Jungling: in *Hot Isostatic Pressing '93*, L. Delaey and H. Tas, eds., Elsevier Sciences B.V., Rotterdam, 1994, pp. 569-80.
75. H.P. Piehler and D.M. Watkins: *Proc. 2nd Int. Conf. on Hot Isostatic Pressing—Theories and Applications*, Gaithersburg, MD, June 1989, ASM INTERNATIONAL, Materials Park, OH, 1991, pp. 321-27.
76. A.M. Laptev, V.N. Samarov, and S.V. Podlesny: *Powder Metall. Int.*, 1990, vol. 22, pp. 23-25.
77. D. Bouvard and M. Lafer: *Advances in Powder Metallurgy*, MPIF, Princeton, NJ, 1989, pp. 491-503.
78. A. Svoboda, L. Bjork, and H.A. Haggblad: in *Computational Methods and Experimental Measurements VII*, GM Carlomagno and CA Brebbia, eds., Computational Mechanics Publications, Southampton, 1994, pp. 29-39.
79. A.G.K. Jinka and R.W. Lewis: *Computer Methods Appl. Mech. Eng.*, 1994, vol. 114, pp. 249-72.
80. M. Khazami-Zadeh, D.G. Seliverstov, F. Petzoldt, and H.D. Kunze: *Powder Metallurgy World Congress*, Les Editions de Physique, Les Ulis, France, 1994, EPMA, Shrewsbury, 1994, vol. I, pp. 761-64
81. V. Skorokhod, E. Olevsky, and M. Shtern: *Sov. Powder Metall.*, 1993, vol. 3, pp. 208-13.
82. A. Svoboda, H.A. Haggblad, and M. Nasstrom: *Eng. Computations*, 1996, vol. 13, pp. 13-39.
83. T.F. Zahrah, F. Charron, and L. Christodoulou: *Powder Metallurgy World Congress*, Les Editions de Physique, Les Ulis, France, 1994, EPMA, Shrewsbury, 1994, vol. I, pp. 783-87.
84. *Proc Int. Workshop on Modelling of Metal Powder Forming Processes*, Grenoble, July 21–23, 1997, organized by Institut National Polytechnique de Grenoble, Universite Joseph Fourier, CNRS, and CEA/CEREM. Available from Professor Bouvard, Directeur du Laboratoire OPM2, ENSPG, Domaine Universitaire, BP46, 38402, Saint Martin-D'Heres Cedex, France.
85. A. Svoboda, H.A. Haggblad, and L. Karlsson: *Computer Methods Appl. Mech. Eng.*, 1997, vol. 148, pp. 299-314.
86. A. Svoboda, L.E. Lindgren, and A.S. Oddy: *Int. J. Num. Methods Eng.*, 1998, vol. 43, pp. 587-606.
87. J.K. McCoy, L.E. Muttart, and R.R. Wills: *Am. Ceram. Soc. Bull.*, 1985, vol. 64, pp. 1240-44.
88. D. Bouvard and M. Lafer: *Powder Metall. Int.*, 1989, vol. 21, pp. 11-15.
89. O. Bouaziz, C. Dellis, and P. Stutz: pp. 67-75 in Ref. 84. *Proc Int. Workshop on Modelling of Metal Powder Forming Processes*, Grenoble, July 21–23, 1997, organized by Institut National Polytechnique de Grenoble, Universite Joseph Fourier, CNRS, and CEA/CEREM. Available from Professor Bouvard, Directeur du Laboratoire GPM2, ENSPG, Domaine Universitaire, BP46, 38402, Saint Martin-D'Heres Cedex, France.
90. K.T. Kim and Y.C. Jeon: pp. 77-86 in Ref. 84. *Proc Int. Workshop on Modelling of Metal Powder Forming Processes*, Grenoble, July 21–23, 1997, organized by Institut National Polytechnique de Grenoble, Universite Joseph Fourier, CNRS, and CEA/CEREM. Available from Professor Bouvard, Directeur du Laboratoire GPM2, ENSPG, Domaine Universitaire, BP46, 38402, Saint Martin-D'Heres Cedex, France.
91. P. Stutz, R. Aryanpour, O. Bouaziz, and C. Dellis: pp. 113-22 in Ref. 84. *Proc Int. Workshop on Modelling of Metal Powder Forming Processes*, Grenoble, July 21–23, 1997, organized by Institut National Polytechnique de Grenoble, Universite Joseph Fourier, CNRS, and CEA/CEREM. Available from Professor Bouvard, Directeur du Laboratoire GPM2, ENSPG, Domaine Universitaire, BP46, 38402, Saint Martin-D'Heres Cedex, France.
92. L. Sanchez, E. Ouedraogo, P. Stutz, and C. Dellis: pp. 295-304 in Ref. 84. *Proc Int. Workshop on Modelling of Metal Powder Forming Processes*, Grenoble, July 21–23, 1997, organized by Institut National Polytechnique de Grenoble, Universite Joseph Fourier, CNRS, and CEA/CEREM. Available from Professor Bouvard, Directeur du Laboratoire GPM2, ENSPG, Domaine Universitaire, BP46, 38402, Saint Martin-D'Heres Cedex, France.
93. C. Dellis, O. Bouaziz, R. Baccino, and F. Moret: pp. 305-14 in Ref. 84. *Proc Int. Workshop on Modelling of Metal Powder Forming Processes*, Grenoble, July 21–23, 1997, organized by Institut National Polytechnique de Grenoble, Universite Joseph Fourier, CNRS, and CEA/CEREM. Available from Professor Bouvard, Directeur du Laboratoire GPM2, ENSPG, Domaine Universitaire, BP46, 38402, Saint Martin-D'Heres Cedex, France.
94. W.B. Eisen, O. Bouaziz, and C. Dellis: pp. 325-34 in Ref. 84. *Proc Int. Workshop on Modelling of Metal Powder Forming Processes*, Grenoble, July 21–23, 1997, organized by Institut National Polytechnique de Grenoble, Universite Joseph Fourier, CNRS, and CEA/CEREM. Available from Professor Bouvard, Directeur du Laboratoire GPM2, ENSPG, Domaine Universitaire, BP46, 38402, Saint Martin-D'Heres Cedex, France.
95. E. Olevsky, S. Van Dyck, L. Froyen, and L. Delaey: *Proc. Int. Conf. on Hot Isostatic Pressing*, May 20–22, 1996, Andover, MA, F.H. Froes, J. Hebeisen, and R. Widmer, eds., ASM, Materials Park, OH, 1996, pp. 63-67.
96. J.M. Duva and P.D. Crow: *Acta Metall.*, 1992, vol. 40, pp. 31-35.

97. W.B. Li and K.E. Easterling: *Powder Metall.*, 1992, vol. 35, pp. 47-52.
98. E. Olevsky, M. Shtern, and V. Skorohod: *Proc. Int. Conf. on Hot Isostatic Pressing*, Antwerp, 1993, L. Delaey and H. Tas, eds., Elsevier Science B.V., Amsterdam, 1994, pp. 45-52.
99. A.G.K. Jinka: *J. Mater. Processing Technol.*, 1996, vol. 57, pp. 382-92.
100. A.L. Maximenko, E.A. Olevsky, Y.A. Panfilov, M.B. Shtern, and E.A. Yurchenko: *Proc. Int. Conf. on Hot Isostatic Pressing*, Antwerp, 1993, L. Delaey and H. Tas, eds., Elsevier Science B.V., Amsterdam, 1994, pp. 61-67.
101. H.N. Wadley, R.J. Schaefer, A.H. Khan, M.F. Ashby, R.B. Clough, Y. Geffen, and J.J. Wlassich: *Acta Metall.*, 1991, vol. 39, pp. 979-86.
102. R.M. McMeeking: *Int. J. Mech Sci.*, 1992, vol. 34, pp. 53-62.
103. J. Besson and M. Abouaf: *Int. J. Solids Struct.*, 1991, vol. 28, pp. 691-702.
104. J. Xu and R.M. McMeeking: *Int. J. Mech. Sci.*, 1992, vol. 34, pp. 167-74.
105. J.K. McCoy and R.R. Wills: *Acta Metall.*, 1987, vol. 35, pp. 577-85.
106. J. Besson and M. Abouaf: *J. Am. Ceram. Soc.*, 1992, vol. 75, pp. 2165-72.
107. R.M. Govindarajan and N. Aravas: *Proc. Int. Conf on Hot Isostatic Pressing*, Antwerp, 1993, L. Delaey and H. Tas, eds., Elsevier Science B.V., Amsterdam, 1994, pp. 29-36.
108. T.F. Zarah, F. Charron, and L. Christodoulou: *Powder Metallurgy World Congress*, Les Editions de Physique, Les Ulis, France, 1994, EPMA, Shrewsbury, 1994, vol. I, pp. 783-87.
109. D. Abondance, R. Baccino, F. Bernier, F. Moret, J.M. de. Monicault, D. Guichard, P. Stutz, and D. Bouvard: *Proc. Powder Metallurgy World Congress*, Les Editions de Physique, Les Ulis, France, 1994, EPMA, Shrewsbury, 1994, vol. I, pp. 797-800.
110. A.G.K. Jinka, M. Bellet, and C. Fourment: *Powder Metallurgy World Congress*, Les Editions de Physique, Les Ulis, France, 1994, EPMA, Shrewsbury, 1994, vol. I, pp. 793-96.
111. E. Olevsky, A. Maximenko, S. Van Dyck, L. Froyen, L. Delaey, and L. Buekenhout: *Int. J. Solids Struct.*, 1998, vol. 35, pp. 2283-303.
112. K.T. Kim, Y.S. Kwon, and H.G. Kim: *Int. J. Mech. Sci.*, 1997, vol. 39, pp. 1011-22.
113. Y.S. Kwon and K.T. Kim: *J. Eng. Mater. Technol.*, 1996, vol. 118, pp. 449-55.
114. Y.S. Kwon and K.T. Kim: *J. Eng. Mater. Technol.*, 1996, vol. 118, pp. 471-77.
115. L.T. Kuhn and R.M. McMeeking: *Int. J. Mech. Sci.*, 1992, vol. 34, pp 563-73.
116. P. Sofronis and R.M. McMeeking: *J. Appl. Mech.*, 1992, vol. 59, pp. 588-95.
117. M.C. Song, H.G. Kim, and K.T. Kim: *Int. J. Mech. Sci*, 1996, vol. 38 (11), pp. 1197-1208.
118. R.E. Dutton, S.L. Semiatin, and R.L. Goetz: *Mater. Sci. Eng. A*, 1996, vol. 221 (1–2), pp. 85-93.
119. S. Schuler, B. Derby, M. Wood, and C.M. Ward-Close: *Key Eng. Mater.*, 1997, vol. 127, pp. 351-58.
120. E. Olevsky, H.J. Dudek, and W.A. Kaysser: *Acta Mater.*, 1996, vol. 44, pp. 707-13.
121. E. Olevsky, H.J. Dudek, and W.A. Kayserr: *Acta Mater.*, 1996, vol. 44, pp. 715-24.
122. M.C. Zhang, M.C. Luo, and F.C. Zeng: *J. Mater. Processing Technol.*, 1997, vol. 72, pp. 262-66.
123. H.P. Buchkremer, R. Hecker, D. Stover, and H. Raes: *Proc 2nd Int. Conf. on Hot Isostatic Pressing: Theory and Applications*, Gaithersburg, MD, June 7–9, 1989, ASM INTERNATIONAL, Materials Park, OH, 1991, pp. 349-54.
124. H.N.G Wadley, A.H Kahn, Y. Geffen, and M. Mester: *Proceedings of Review of Progress in Quantitative Nondestructive Evaluation*. D.O. Thompson and D.E. Chiment, eds., Plenum, New York, NY, 1988, vol. 7B, pp. 1589-98.
125. A.H. Kahn, M.A. Mester, and H.N.G. Wadley: *Proc 2nd Int. Conf. on Hot Isostatic Pressing; Theory and Applications*, Gaithersburg, MD, June 7–9, 1989, ASM INTERNATIONAL, Materials Park, OH, 1991, pp. 341-48.
126. R.J. Schaefer and G.M. Janowski: *Acta Metall. Mater.*, 1992, vol. 40, pp. 1645-51.
127. D.A. Stubbs and R.E. Dutton: *JOM*, 1996, vol. 48, pp. 29-31.
128. H.R. Piehler and D.P. DeLo: *Progr. Mater. Sci.*, 1997, vol. 42, pp. 263-76.
129. R.M. German and A. Bose: *Mater. Sci. Eng.*, 1989, vol. A107, pp. 107-16.